This document is the accepted manuscript version of the following article:
Xu, X., Xia, X., Zhang, K., Rai, A., Li, Z., Zhao, P., Wei, K., Zou, L., Yang, B., Wong, W. K., Chiu, P. W. Y., & Bian, L. (2020). Bioadhesive hydrogels demonstrating pH-independent and ultrafast gelation promote gastric ulcer healing in pigs. Science Translational Medicine, 12(558), eaba8014 (15 pp.). https://doi.org/10.1126/scitranslmed.aba8014

Bioadhesive hydrogels demonstrating pH-independent and ultrafast gelation promote gastric ulcer healing in pigs

Xiayi Xu[1†], Xianfeng Xia[2, 3†], Kunyu Zhang[1, 4†], Aliza Rai[5], Zhuo Li[1], Pengchao Zhao[1], Kongchang Wei[1, 6], Li Zou[7], Boguang Yang[1], Wai-Ki Wong[1], Philip Wai-Yan Chiu[1, 3, 5*], Liming Bian[1, 8*]

[1] Department of Biomedical Engineering, The Chinese University of Hong Kong, Hong Kong SAR 999077, China.
[2] Department of Endoscopy, State Key Laboratory of Oncology in South China, Sun Yat-sen University Cancer Center, Guangzhou 510000, China.
[3] Chow Yuk Ho Technology Centre for Innovative Medicine, The Chinese University of Hong Kong, Hong Kong SAR 999077, China.
[4] Department of Materials Science and Engineering, Johns Hopkins University, Baltimore, MD 21218, USA.
[5] Department of Surgery, Institute of Digestive Disease, State Key Laboratory of Digestive Disease, The Chinese University of Hong Kong, Hong Kong SAR 999077, China.
[6] Empa, Swiss Federal Laboratories for Materials Science and Technology, Laboratory for Biomimetic Membranes and Textiles, Lerchenfeldstrasse 5, CH-9014 St. Gallen, Switzerland.
[7] Department of Orthpaedics and Traumatology, The Chinese University of Hong Kong, Hong Kong SAR 999077, China.
[8] The Chinese University of Hong Kong, Shenzhen Research Institute, Shenzhen 518000, China.

[†]These authors contributed equally to this work.

*Corresponding author. Email: philipchiu@surgery.cuhk.edu.hk; lbian@cuhk.edu.hk;

Single-sentence summary:
Bioadhesive hydrogel with ultrafast gelation independent of environmental pH is endoscopically delivered to enhance gastric ulcer healing.

Abstract

Hydrogels are soft materials used in an array of biomedical applications. However, the in situ formation of hydrogels at target sites, particularly in dynamic in vivo environments, usually requires a prolonged gelation time and results in poor adhesion. These limitations cause considerable loss of both hydrogel mass and encapsulated therapeutic cargoes, thereby compromising treatment outcomes. Herein we report the development of a hydrogel based on thiourea–catechol reaction to enhance the bioadhesion. Compared with classical bioadhesive hydrogels, our hydrogels show enhanced mechanical properties, exceedingly short curing time, and pH-independent gelation with a much lower oxidant concentration. We further report the robust adhesion of our hydrogels to acidic gastric tissues and easy delivery to the porcine stomach via endoscopy. The delivered hydrogels adhered to ulcer sites in vivo for at least 48 hours. Hydrogel treatment of gastric ulcers in rodent and porcine models accelerated ulcer healing by suppressing inflammation and promoting re-epithelization and angiogenesis. The improved retention of pro-regenerative growth factors and reduced exposure to external catabolic factors after hydrogel application may contribute to the observed therapeutic outcomes. Our findings reveal a promising biomaterial-based approach for treating gastrointestinal diseases.

INTRODUCTION

Hydrogels are promising biomaterials for medical applications (*1-6*). In situations when direct placement of hydrogels is inaccessible, in situ hydrogel formation is desirable (*7-10*). Prolonged gelation time and insufficient adhesion to the target site after gelation can lead to loss of hydrogel volume and subsequent loss of therapeutic cargo (*11, 12*), particularly in a fluidically, chemically, and mechanically dynamic environment in vivo. These features may compromise treatment outcomes, thus limiting the broad application of hydrogels. The development of instant-gelation hydrogels with strong in situ adhesion under complex chemical and mechanical environments is therefore critically important (*13*).

Catechol (Cat)-based hydrogels have been reported to form quickly (within minutes) under alkaline conditions (*14-17*). Notably, by mimicking a typical amino acid in mussel foot proteins (mfps), namely, 3,4-dihydroxyphenylalanine (DOPA) (*18*), many Cat-related hydrogels show strong adhesion to both organic and inorganic surfaces (*19-24*). However, catechol inevitably undergoes oxidation to quinone when exposed to oxidants such as O_2, resulting in a loss of adhesiveness (*25, 26*). Inspired by the thiol-rich mfp-6, which rescues the loss of adhesion by minimizing the auto-oxidation of DOPA (*27*), we have previously demonstrated the use of the reducing thiourea group (abbreviated as NCSN, the four major atoms in thiourea) to preserve the adhesiveness of mfp-mimicking hydrogels (*28*).

In this work, we report a bioadhesive hydrogel formed via NCSN–Cat reaction with ultrafast gelation properties independent of the environmental pH (Fig. 1A). Simple mixing of the polymer precursor solution with the oxidant solution led to the ultrafast formation of hyaluronic acid (HA)-Cat-NCSN hydrogels with enhanced mechanical properties and reduced oxidant dosage required for gelation compared with classical catechol-based hydrogels prepared via catechol–catechol reactions (*29*). By spraying the oxidant solution on top of the precursor solutions, the resulting HA-Cat-NCSN hydrogels exhibited strong adhesion and retention on wet and acidic inorganic or tissue surfaces (Fig. 1B).

With the ability to adhere to the target site after ultrafast gelation even in an acidic

and mechanically dynamic environment, our hydrogels can be used in the gastrointestinal (GI) tract. Chronic peptic ulcers (PUs) can be treated by medications such as proton pump inhibitors (PPIs). However, an increasing number of clinical studies have shown that chronic use of PPIs is associated with complications, leading to concerns about drug safety (*30*). Furthermore, the artificial ulcers induced by endoscopic submucosal dissection (ESD) after removal of early gastric cancer have high risk of post-operative bleeding and re-bleeding even a few days after surgery, which increase the morbidity and mortality of patients. So far, there is no recommended endoscopic approach for treatment of ESD-induced ulcers and ulcer-related complications. Therefore, the development of a bioadhesive biomaterial that can gel rapidly under acidic environment in the stomach and can be endoscopically delivered to target sites is of have high clinical importance for the prevention of ulcer-related complication and the promotion of GI mucosal healing (*31, 32*). Here, we tested the feasibility of delivering hydrogel precursors and curing agents through endoscopic catheters to induce in situ gelation at ulcer sites in a porcine model and further evaluated the therapeutic benefits of HA-Cat-NCSN hydrogels in rodent and porcine models. We also investigated the possible mechanism by which the hydrogels promote ulcer healing, via catechol-mediated hydrogel–macromolecule interactions. By easy endoscopic delivery, our hydrogels offer a clinically feasible and effective therapeutic approach for treating gastric diseases.

RESULTS

pH independence, fast gelation, and superior physical properties of HA-Cat-NCSN hydrogels

We synthesized the precursor polymers, HA-NCSN and HA-Cat, based on our previously reported protocols (*17, 28*). The degree of substitution (D.S.) of NCSN and catechol on HA was about 35% and 48%, respectively (fig. S1 and S2). Detailed descriptions of the methods used to prepare and characterize the modified polymers are presented in the Supporting Information. Ultraviolet-visible (UV-Vis) spectroscopy was used to track the change in Cat during the reaction process as a method to investigate

the gelation mechanism. For HA-Cat, the quinone peak (λ_{max}=395 nm) appeared immediately after the addition of $NaIO_4$, indicating the rapid oxidation of Cat in the presence of oxidants (Fig. 2A). The addition of HA-NCSN reverted the quinone to Cat, as evidenced by a reduction in the quinone peak (Fig. 2B, blue array). The reduction in the quinone peak was accelerated by adding an increased amount of HA-NCSN or replacing HA-NCSN with excess amounts of *N*, *N*'-dimethylthiourea (Fig. 2C and fig. S3). The UV-Vis spectroscopy result was consistent with our hypothesis that the NCSN group reduces oxidized Cat (quinone) to Cat, thereby preserving the bio-adhesiveness of hydrogels.

Consistent with previous reports showing that the formation of HA-Cat hydrogels depends on the pH (*33, 34*), a 2% HA-Cat solution formed a hydrogel in 30 min at pH 7, but the process required a much longer time (about 3 h) at pH 2. When the molar ratio of the oxidation agent ($NaIO_4$) to Cat was decreased from 1:1 to 0.1:1, the HA-Cat precursor solution was unable to form a hydrogel (Fig. 2D). In contrast, at this reduced amount of oxidant, the mixture of 1% HA-Cat and 1% HA-NCSN formed hydrogels within 5 seconds, independent of pH. The immediate gelation of the mixture of HA-Cat and HA-NCSN with low concentration of oxidant at pH 2 was also evidenced by the higher G' value than G'' value upon starting the rheology measurement. By contrast, the mixture of HA-Cat and low concentration oxidant solution maintained sol-like behavior during the rheology test of the same duration (G''>G') (fig. S4A). The ability to induce gelation with a much lower dosage of strong oxidants, such as $NaIO_4$, improved the biocompatibility and therefore increased the translation potential of our hydrogels. The HA-Cat-NCSN hydrogels remained transparent and colorless, whereas HA-Cat hydrogels turned brown after gelation due to quinone formation, indicating that the Cat in the HA-Cat-NCSN hydrogels remained largely unoxidized (Fig. 2D). This ultrafast hydrogel formation independent of pH was attributed to the low pK_a of the thiourea derivatives (pK_a=-1) (*35*) and its ability to attack Cat as a strong nucleophile (*36*).

According to the results of the time sweep rheological analysis, HA-Cat-NCSN

hydrogels displayed a significantly higher storage modulus (G') (4.5-, 4.3-, and 4.0-fold higher with $P < 0.001$, $P < 0.01$ and $P < 0.01$ at pH 2, 4, and 7, respectively) than HA-Cat hydrogels prepared under the same conditions (Fig. 2E and fig. S4, B and C). The significant differences in the mechanical properties of the hydrogels may be attributed to differences in the gelation mechanism. For HA-Cat hydrogels, crosslinking depends on the oligomerization of oxidized Cat (quinone) groups (*14, 15, 29*). However, due to the random nature of the Cat oligomerization reaction (*15*), the crosslinks in HA-Cat hydrogels are irregular. In contrast, the highly efficient Cat-thiourea coupling leads to an equimolar reaction between NCSN and Cat, thereby yielding a more uniform crosslinked structure in the HA-Cat-NCSN hydrogels (*35*). These findings are consistent with our recent study showing that hydrogels containing dimerized Cat crosslinks exhibit stronger mechanical properties than the hydrogels crosslinked by Cat oligomerization (*37*).

The mechanical properties of HA-Cat-NCSN hydrogels were further investigated by varying the pH and the amount of $NaIO_4$ added. Both G' and G'' increased with increasing concentration of $NaIO_4$; however, the pH value did not affect the rheological properties (also shown in the strain sweep data presented in fig. S5A), thereby confirming the pH-independence of HA-Cat-NCSN hydrogel formation (Fig. 2F and fig. S5B). Based on the results of the compression test, the stress at fracture reached about 30 kPa with a fracture strain of 75%, even when the $NaIO_4$: Cat ratio was reduced to 0.1 (Fig. 2G). Meanwhile, the HA-Cat-NCSN hydrogels prepared at the same pH changed from the colourless and transparent appearance to become brownish with increasing $NaIO_4$/catechol molar ratio, and, this indicated the preservation of unoxidized catechol groups at low oxidant concentration (fig. S5C). The degradation of HA-Cat-NCSN hydrogels was only slightly faster in acidic buffer than that in pH=7 buffer (Fig. 2H). Therefore, unlike HA-Cat hydrogels, HA-Cat-NCSN hydrogels can be prepared with ultrafast gelation, a low oxidant concentration, and a wide range of pH values, and they possess improved mechanical properties.

In situ ultrafast gelation and robust adhesion of HA-Cat-NCSN hydrogels in vitro.

Besides using chemical oxidant, the gelation of HA-Cat-NCSN hydrogels also can be induced by oxidizing enzymes such as mushroom tyrosinase (MT) (*38, 39*). By tuning the enzyme concentration, we prepared hydrogels with controllable gelation times. The gelation time increased from 2-4 seconds to more than 30 min when the MT concentration was decreased from 2000 to 50 units/ml (Fig. 3A). Additionally, the mechanical properties of the enzyme-induced hydrogels were similar to those of the oxidant-induced hydrogels (fig. S6A). We prepared more uniformly-crosslinked adhesive hydrogels between glass slides for lap shear testing (*40*) by using low concentration MT to slow gelation and minimize the testing artefacts due to uneven rapid gelation. The lap shear test revealed that the adhesion strength of HA-Cat-NCSN hydrogels was significantly higher than that of HA-Cat hydrogels ($P < 0.05$, fig. S6B). The adhesion strength of HA-Cat-NCSN hydrogels decreased after PBS incubation, however, the differences in the adhesion strength among hydrogels incubated in PBS at different time points (1 min, 10 min, and overnight) were not significant ($P > 0.05$, Fig. 3B). Thus, the adhesion of HA-Cat-NCSN hydrogels can be maintained even under swollen and wet conditions.

The fast gelation of HA-Cat-NCSN hydrogels helps reduce the loss of un-crosslinked polymers and promotes the retention of hydrogels in a fluidically and mechanically dynamic environment (*11*). Firstly, a mixture of HA-Cat and HA-NCSN was directly pipetted into $NaIO_4$ solutions (~0.048% w/v). This led to the rapid formation of thread-like hydrogels (Fig. 3C). Furthermore, an acidic precursor solution (pH 2) containing a mixture of HA-Cat and HA-NCSN was deposited onto glass to analyse the rapid in situ formation of HA-Cat-NCSN hydrogels. A low concentration of $NaIO_4$ (~0.048% w/v) was then sprayed on top of the precursor solution, resulting in immediate gelation. After immersion in acidic buffer for 15 min, the hydrogel remained firmly attached to the glass surface. In contrast, the pure HA-Cat precursor solution did not form a hydrogel, even after being sprayed with a high concentration of $NaIO_4$ (~1.0% w/v) (Fig. 3D).

These results consistently show that HA-Cat-NCSN hydrogels have an ultrafast gelation rate in an acidic and wet environment. We believe that this property makes the hydrogels ideal for treating challenging clinical conditions. For example, in the harsh

stomach internal environment, the constant production of gastric acid and physical forces due to gastric motility hamper the formation and retention of protective and therapeutic coverings on ulcers, thereby impeding ulcer healing. Therefore, it is highly desirable to develop a biomaterial that can fit into the ulcer site, adhere firmly under acidic condition in the presence of mechanical agitation, and provide protection against catabolic factors to promote ulcer healing.

To evaluate the bioadhesion of HA-Cat-NCSN hydrogels, lap shear testing was conducted by coating the surface of both glass slides with porcine gastric tissues (fig. S7A). The results showed that after incubation in the acidic gastric medium overnight, the strength of hydrogel-mediated adhesion between gastric tissue-coated glass slides was similar to that of the bare glass slides (fig. S7B). To further demonstrate the adhesion of our hydrogels on gastric tissues, a mixture of HA-Cat and HA-NCSN was applied on fresh pig gastric tissue ex vivo, which had been pre-soaked in acidic gastric medium (pH 2) for 1 hour. The results showed that gelation occurred within a few seconds after spraying the oxidant. The hydrogels formed in situ showed strong adhesion to the wet gastric surface, as evidenced by the capability to withstand excessive stretching and twisting of the gastric tissue (Fig. 3E and movie S1). After soaking the hydrogel-bearing tissue in gastric medium for another 30 min, the adherent hydrogels were still able to withstand mechanical challenges without detaching from the tissue surface. Attempts to peel the hydrogel from the tissue surface resulted in a large amount of hydrogel remaining on the tissue, indicating the robust bio-adhesion of our hydrogels (Fig. 3E). Such a strong wet adhesion of HA-Cat-NCSN hydrogels to tissues can be attributed to the high reactivity of abundant catechol groups (preserved by the NCSN groups) on the polymer network to various natural nucleophiles (e.g., amido bond, thiol and amines) (*14, 19*) that are present on the protein of tissue surface.

The HA-Cat-NCSN hydrogels promote ulcer healing in a rodent model

We evaluated the efficacy of HA-Cat-NCSN hydrogels to treat gastric ulcers in a rodent model. Two kissing gastric ulcers were induced in each rat by infusing an acetic acid solution into a hollow O-ring mold inserted in the stomach (n=6 rats) (Fig. 4A) (*41*).

The ulcer on the anterior wall of the stomach was sprayed with the hydrogels (hydrogel group), whereas the ulcer on the posterior wall served as the control without any intervention (control group). On day 7 post-operation, a macroscopic examination of the harvested stomach tissues revealed a significantly smaller ulcer area in the hydrogel group than that in the control group (Fig. 4, B and C; fig. S8A) (Hydrogel group: 0.099 ± 0.029 cm^2 *vs*. Control group: 0.203 ± 0.065 cm^2; $P < 0.05$). Haematoxylin and eosin (H & E) staining showed severe oedema in the ulcer base of the control group compared to the hydrogel group (Fig. 4D). The infiltration of neutrophil (fig. S8B; green arrowhead) and lymphocytes (fig. S8B; red arrowhead) (*42*), which represents inflammation at the ulcer site, was significantly decreased at the ulcers receiving hydrogel treatment compared with the controls on day 7 ($P < 0.05$, Fig. 4E). We also evaluated angiogenesis and re-epithelization, key factors contributing to gastric ulcer healing (*43*), in ulcers treated with or without hydrogels. Immunostaining for CD31 (endothelial cell marker) showed a significantly greater density of capillaries at the submucosa of ulcers treated with hydrogels ($P < 0.01$, Fig. 4, F and G). Similarly, more positive staining for proliferating cell nuclear antigen (PCNA), a proliferation marker of G1/S phase, was found at the areas of ulcer base and around the margin (base / margin area indicated in fig. S8C) in the hydrogel group compared with the control group (Fig. 4H). Collectively, these results suggest that application of the HA-Cat-NCSN hydrogel on ulcer defects accelerated the healing of gastric ulcers by suppressing inflammation, promoting capillary regeneration, and enhancing cell proliferation.

Endoscopically delivered HA-Cat-NCSN hydrogels firmly adhere to gastric ulcers in vivo in pigs

The feasibility of delivering soluble hydrogel precursors and curing agents through an endoscopic catheter to induce in situ gelation at the ulcer sites is of great clinical interest. Endoscopic delivery of hydrogels serves as an important simulation to clinical practice and is ideal for providing instant protection of gastric wound and further promoting ulcer healing after ESD procedure. To demonstrate this capability, two artificial gastric ulcers were created in porcine stomach by ESD (fig. S9**)**. A mixture of precursor of HA-

Cat and HA-NCSN was applied topically onto the ulcer base in the treatment group using an endoscopic catheter (channel 1), followed immediately by spraying the oxidant solution through another endoscopic catheter (channel 2) to induce the rapid in situ gelation (Fig. 5A). The control group only received ESD with no hydrogel treatment. After 24 hours, endoscopic surveillance revealed the persistent adhesion of the HA-Cat-NCSN hydrogels to the ulcer base, despite the partial loss of the upper layer (Fig. 5B). 48 hours after the endoscopic operation, gastric tissue was harvested for histological processing. Hydrogels remained on the wound area as evidenced by blue dye (Fig. 5C). Immunohistochemical staining for inducible nitric oxide synthase (iNOS)(*44*), a marker of inflammation, showed less iNOS expression at the ulcer sites covered with the hydrogels when compared with the control(fig. S10). These results hence revealed that our hydrogels could firmly adhere to the gastric ulcer sites in living pigs for at least 48 h, despite the excessive gastric motility, acidic pH, and harsh bio-fluidic environment in vivo.

The HA-Cat-NCSN hydrogels promote ulcer healing in a porcine model

We compared the therapeutic efficacy of hydrogel treatment with the available drug sucralfate for gastric ulcer healing in the porcine model. Three artificial gastric ulcers were created by ESD in each pig (n=3 pigs). Hydrogels and sucralfate were delivered through endoscopic catheters and applied on the respective ulcers on day 0 and day 7 (hydrogel group and drug treatment group); the third ulcer in each pig served as the control without any treatment (control group) (Fig. 6A and fig. S11). Endoscopic surveillance was performed every week to assess the ulcer healing process until euthanasia on day 14 for sample collection. The ulcer index (longest radius × shortest radius of the ulcer) of the hydrogel group was significantly smaller than that of the control group on day 7 ($P < 0.05$) and 14 ($P < 0.05$) whereas the difference between the control group and drug treatment group on day 14 was not significant ($P > 0.05$, Fig. 6, B and C). H&E staining of ulcer tissues showed obvious regenerative epithelium at the ulcer base in the hydrogel group on day 14 (Fig. 6D). Drug treatment also induced

epithelium regeneration, but the structure of the glands was quite distorted. There was very little epithelium regeneration in the ulcer base of the control group on day 14. Histological evaluation showed that neutrophil and lymphocyte infiltration, as well as the ulcer margin height, were significantly reduced in the hydrogel group compared with the control group on day 14 ($P < 0.05$) (Fig. 6, E and F). More regenerative epithelium with normal morphology and higher density of granulation tissue was also observed in the hydrogel group compared with the control group on day 14 ($P < 0.01$, $P < 0.05$ respectively) (Fig. 6, G and H). However, the scoring of ulcer margin height and granulation tissue thickness was not significantly different between the drug treatment group and control group on day 14 ($P > 0.05$).

To assess neovascularization after hydrogel treatment, double immunofluorescence staining against CD31 and α-smooth muscle actin (α-SMA) was performed and the results showed significant increase of the densities of capillaries ($P < 0.05$) and small arteries ($P < 0.001$) in the granulation tissues in the hydrogel group compared with control group on day 14 (Fig. 7, A to C). PCNA staining also indicated that the number of positive cell nuclei was significantly higher at areas of ulcer base and around the margin in the hydrogel group compared with the drug treatment group ($P < 0.05$) and the control group ($P < 0.001$) respectively (Fig. 7, D and E). Furthermore, hydrogel application induced overexpression of genes responsible for the wound healing in the ulcer samples collected on day 7 (Fig. 7F). The PCR array data showed that *PTGS1* (prostaglandin-endoperoxide synthase 1), *IGF-1*(insulin-like growth factor 1), *EGF* (epidermal growth factor), *EGFR* (epidermal growth factor receptor), *VEGFA* (vascular endothelial growth factor A), *IL10* (interleukin 10), *TGFα* (transforming growth factor, alpha), *MMP-7* (matrix metallopeptidase 7) and *MMP-9* were up-regulated after hydrogel treatment compared with the controls. These genes are known to mediate cellular events critical to ulcer healing including re-epithelization, neovascularization, anti-inflammation, and tissue remodelling (*45-48*). Drug treatment showed less impact on gene expression, but *CSF2* and *PTGS2* were increased compared with the hydrogel group, which suggests the mechanisms of hydrogel and sucralfate treatment for ulcer healing might differ. In this study, the therapeutic efficacy in the drug treatment group

was achieved on the basis of precise delivery of Sucralfate to the ulcer site through an endoscopic clamp, whereas the practical oral administration of Sucralfate adopted by patients cannot guarantee such efficient delivery of drug and may therefore cause inferior therapeutic outcome. Taking these findings together, we believe that our HA-Cat-NCSN hydrogel treatment is comparable or even superior to traditional drug treatment in promoting gastric ulcer healing.

Mechanism of ulcer healing via molecular sequestration of HA-Cat-NCSN hydrogels

The mechanism underlying the enhanced ulcer healing by the hydrogel treatment is complex. As a bioactive biopolymer, hyaluronic acid itself can improve ulcer healing (*49*). In this study, live/dead cell staining revealed that the majority of human gastric epithelial cells (GES-1 cell line) (~89%) and human mesenchymal stem cells (hMSC) (~93%) encapsulated in HA-Cat-NCSN hydrogels remained viable after 7 days of culture, thereby confirming the cytocompatibility of our hydrogels (fig. S12, A and B). As shown in previous studies (*50*), catabolic factors present in the gastric juice that are activated by low pH (≤3), such as pepsin, are responsible for exacerbating ulcerated mucosa and hindering healing by degrading pro-regenerative factors, including basic fibroblast growth factor (bFGF), which are required to promote angiogenesis and accelerate ulcer healing. Meanwhile, hydrogels bearing catechol groups are known to capture biomacromolecules by reacting with the nucleophile groups. Therefore, we hypothesize that the HA-Cat-NCSN hydrogels may restrict macromolecule transport and reduce the exposure of ulcer sites to catabolic enzymes in gastric juice, promoting the accumulation of cell-secreted pro-regenerative factors at ulcer sites that facilitates the ulcer healing process (Fig. 8A). We adopted a transwell system to test the ability of hydrogels to restrict catabolic enzymes. A layer of HA-Cat-NCSN hydrogel or non-adhesive hydrogel (methacrylated hyaluronic acid hydrogel, i.e., MeHA hydrogel) with the same polymer content was formed at the bottom of upper chamber, to which the pepsin solution was added (fig. S13). Because the pepsin concentration in stomach falls in the range of 0.5-1.0 mg/ml(*51*), here we used 2 mg/ml pepsin dissolved in pH 3 buffer.

Over 7 days, HA-Cat-NCSN hydrogels significantly reduced the diffusion of pepsin from the upper chamber into the lower chamber when compared with the MeHA hydrogel group and no hydrogel group ($P < 0.05$ and $P < 0.001$, respectively). On day 7, only 45% of the total pepsin diffused through the HA-Cat-NCSN hydrogels, whereas 68% and 85% of the total pepsin diffused through MeHA hydrogels and the upper chamber without hydrogel coating, respectively (Fig. 8B). In addition, we used a model protein, bovine serum albumin (BSA), to test the protein accumulation in the hydrogels. After 24 hours of incubation in BSA solution, HA-Cat-NCSN hydrogels accumulated significantly more BSA compared with MeHA hydrogels (HA-Cat-NCSN: 230 μg/mg *v.s.* MeHA: 103 μg/mg, $P < 0.001$; Fig. 8C). When BSA was encapsulated in the hydrogels, HA-Cat-NCSN hydrogels showed significantly less initial burst release ($P < 0.001$ at 24 hours) and more sustained release of BSA than MeHA hydrogels (fig. S14). These results together indicated the superior capability of HA-Cat-NCSN hydrogels for protein retention in vitro. To mimic the situation in vivo of pro-regenerative factors retained by HA-Cat-NCSN hydrogels, GES-1 cells were cultured either in bFGF-supplemented medium, with a bFGF-encapsulated hydrogel or with a bFGF pre-adsorbed hydrogel in medium for 4 hours. Culture medium in all groups was subsequently replaced with fresh medium, and cells were further cultured for 7 days. Compared with FGF group (bFGF supplementation), cells co-cultured with the FGF-encapsulated or FGF pre-adsorbed hydrogels exhibited significantly more proliferation over 7 days ($P < 0.0001$, Fig. 8, D and E). Maeng *et al.* (*32*) previously reported an epidermal growth factor (EGF)-loaded hydrogel for promoting ulcer healing. Here, we demonstrate that our HA-Cat-NCSN hydrogels formed in situ can retain the pro-regenerative endogenous growth factors and limit the exposure to catabolic factors (e.g., pepsin) via molecular sequestration in vitro, and this property may be related to the promotion of ulcer healing effect after hydrogel treatment observed in the animal experiments in vivo.

DISCCUSSION

In this work, we report a bio-inspired bioadhesive HA-Cat-NCSN hydrogel with ultrafast gelation independent of environmental pH. Distinct attributes enable our bioadhesive hydrogels to meet the complex and stringent requirements for potential clinical applications, especially for treating GI tract disorders such as peptic ulcers. Because in situ gelation is widely acknowledged to enhance the interaction between hydrogels and tissues (*52*), we induced in situ gelation of HA-Cat-NCSN hydrogels in the stomach by delivering the precursor and oxidant through separate endoscopic catheters. The instantly formed hydrogels were capable of adhering to gastric ulcer sites, providing a protective barrier for at least 48 hours regardless of the excessive gastric motility, acidic pH, and harsh biofluidic environment in the stomach of pigs, leading to enhanced ulcer healing. This endoscopically-assisted in situ gelation method can provide surgeons with more control over the treatment process and causes minimal disruption to the current clinical procedures.

The promising application of HA-Cat-NCSN hydrogels could be further expanded in the future. For example, acute gastric bleeding is a life-threatening complication of gastric disease. Fatal gastric arterial haemorrhage can happen during endoscopic surgery, and there are few effective treatments available (*53*). Although commercial haemostatic powders for stopping acute gastric bleeding endoscopically have been reported (*31, 54*), these powders have limitations that may restrict their widespread clinical use. In particular, the gels formed by the powders lack sufficient adhesion to the ulcer and can be washed away within hours, and this not only limits the therapeutic efficacy but also causes potential risk of biliary orifice obstruction, allergic reaction, and choking. Furthermore, dispensing the powder to ulcers can severely block endoscopic observation and the acidic stomach environment often impede the gelation of powders based on Schiff base crosslinking (*31*). The endoscopic delivery of our HA-Cat-NCSN hydrogels and their quick solidification under acidic environments would be highly desirable for arresting acute gastric bleeding. Since our hydrogels can considerably accelerate the healing process of ulcers caused by ESD, the application of hydrogels in situ may also reduce the incidence of acute gastric bleeding after the ESD

procedure. Nevertheless, to achieve good haemostasis, especially for arterial haemorrhage with high burst pressure, further modification and haemostasis evaluation of our hydrogels for such applications should be pursued in future studies.

Our study has several limitations. The catechol-based hydrogels have been reported to achieve controlled drug release via the interactions between catechol and drugs (*55, 56*). However, the capability of HA-Cat-NCSN hydrogels to mediate sustained drug delivery to further boost their therapeutic effect remains to be investigated in future studies. Additionally, repeated endoscopic delivery of hydrogels may result in reduced patient compliance. Switching to conventional oral administration of ulcer-healing drugs after the first endoscopic delivery of hydrogels will likely be more practical to achieve better patient compliance, whereas the repeated hydrogel treatments could be a valuable alternative for a subgroup of patients with poor record of compliance to routine and long-term multi-drug regimens. Furthermore, the sample size of the pig study is small. Nevertheless, the observations from the pig study were consistent with those results from rodent studies. Future large animal studies with larger sample sizes and longer follow-up duration are needed before clinical translation.

In summary, we developed a bio-inspired hydrogel based on thiourea-Cat coupling between the NCSN (thiourea) and Cat groups grafted to HA backbone. The presence of the reducing NCSN groups helped reduce the excessive oxidization of Cat, thus preserving the adhesiveness of the hydrogels. Such hydrogels exhibited ultrafast gelation independent of pH, and simply spraying a low concentration of oxidant on top of the precursor achieved rapid in situ formation of stable and adhesive hydrogels. The hydrogel could be applied to the GI lumen where the internal environment is relatively complex and challenging due to the secretion of digestive juice and constant gastric movements. Here, our data show that HA-Cat-NCSN hydrogels could be endoscopically delivered to the target ulcer site in the stomach of the pig and retained in situ for at least 48 hours. As a protective barrier formed at the ulcer surface to impede the infiltration of external catabolic factors and to accumulate growth factors around ulcer area, our hydrogels promoted the ulcer healing process in both rodent and porcine models through suppression of inflammation and promotion of neovascularization and

cellular proliferation. The therapeutic efficacy of our hydrogels was comparable to the drug treatment (sucralfate) group, suggesting that it is a promising alternative for the treatment of refractory ulcers in clinical scenarios.

MATERIALS AND METHODS

Study design

The objective of this study was to develop a bio-inspired bioadhesive hydrogel with pH-independent and ultrafast gelation for treating gastric ulcers. The structure of synthesized polymers and hydrogel crosslinking mechanism was examined by UV-Vis spectroscopy analysis. The mechanical properties of the obtained hydrogels and classical HA-Cat hydrogels were examined by rheological tests. In vitro gelation demonstrations were designed to show the ultrafast gelation of the bioadhesive hydrogels on different substrates and in solutions. In vitro molecular sequestration experiments were designed to test the proposed mechanism of hydrogel-assisted ulcer healing. All experiments in vitro were repeated at least three times. Animal studies were assigned with a self-controlled design. For the rat study, two gastric ulcers were created in each animal; one ulcer was treated with hydrogel as the experimental group, whereas the other ulcer served as the control without any treatment. For the large animal study in porcine model, three gastric ulcers were induced in each pig; one ulcer was sprayed with hydrogel via endoscope as the experimental group, one was treated with sucralfate (500 mg/ulcer) as the positive control group, and the third one served as the control without any treatment. Follow-up endoscopic surveillance was performed every week during the 14-day period to evaluate ulcer healing and an endoscopic ruler was used to measure the ulcer size. The sample size of animal studies was estimated based on our experience using the animal models and the power calculation (effect size = 1.2 for rat study and 1.58 for pig study, α=0.05, power = 0.80) (*41, 57*). Blinded approach was used for the histopathological evaluation and analysis of immunohistochemistry and immunofluorescence images. Original data were reported in data file S1.

Synthesis and characterization of HA-Cat

The quaternary ammonium salt of sodium hyaluronate (HA-TBA) was initially synthesized as a pre-conjugate. HA (NaHa, 160 kDa, Shengjiade Biotechnology Co., Ltd.) was dissolved in DI water at a concentration of 1% (w/v). Dowex 50W (J&K Scientific) was then added to the solution at a concentration of 3% (w/v) and stirred for 7-8 h at room temperature. Tetrabutylammonium hydroxide (TBAOH, 0.4 M, J&K Scientific) was added to neutralize the solution. The solution was then frozen and lyophilized for approximately 4 days to obtain a dry product. Afterwards, HA-Cat was synthesized by conjugating dopamine hydrochloride (J&K Scientific) to HA-TBA using 4-dimethylaminopyridine (DMAP, Aladdin) and DIPEA. HA-TBA (0.5 g) was dissolved in 50 ml of Dimethylformamide (DMF, Fisher Scientific), and then hydroxybenzotriazole (HOBt, J&K Scientific) and N,N-diisopropylcarbodiimide (DIC, J&K Scientific) were added at molar ratios of 2.5:1 and 0.5:1, respectively, to HA-TBA and stirred for 4 h under a nitrogen atmosphere. After stirring, dopamine hydrochloride and DMAP were added to the solution at a 0.5:1 molar ratio to HA-TBA, and DIPEA was added at a molar ratio of 2.5:1 to HA-TBA. The mixture was stirred for another 24 h. Unreacted dopamine and other chemicals were removed through dialysis against acidic NaCl (pH 4) for 3 days and DI water for 3 days. The purified solution was then frozen, lyophilized, and stored at 4°C until use. The degree of substitution (DS) of Cat was confirmed by ^{1}H NMR (Bruker Advance 400 MHz spectrometer).

Synthesis and characterization of HA-NCSN

HA was first converted to HA hydrazide (HA-ADH). Briefly, 1 g of HA was dissolved in 200 ml of DI water. Then, 2.396 g of N-(3-dimethylaminopropyl)-N'-ethylcarbodiimide hydrochloride (EDC, J&K Scientific), 1.914 g of HOBt, and 34.84 g of adipic dihydrazide (ADH, J&K Scientific) were added. The solution was stirred for 6 h. NaOH was constantly added to the solution during stirring to maintain a pH of approximately 6.8. The solution was then dialysed against NaCl for 3 days and DI water for 3 days. The purified solution was frozen and lyophilized to obtain a dry product. For the synthesis of HA-NCSN, HA-ADH was dissolved in DI water at a concentration

of 1% (w/v). Then, five-fold excess methyl isothiocyanate (CH_3NCS, J&K Scientific) compared with HA-ADH was dissolved in DMSO, added to the HA-ADH solution, and stirred for 3 days under a nitrogen atmosphere. The mixture was further purified through dialysis against NaCl for 3 days and DI water for another 3 days. ^1H NMR spectroscopy of the product was conducted to confirm the DS of the residue.

Mechanical properties

The mechanical properties of HA-Cat hydrogel and HA-Cat-NCSN hydrogel were measured on a rotating rheometer (Anton Paar MCR301). The dynamic moduli (G' and G'') of hydrogel samples were obtained, and the strain and frequency were maintained at constant values of 1% and 1 Hz, respectively. Strain sweeps were obtained by varying the strain from 0.1% to 100%. For compression testing, hydrogel samples were compressed at a fixed rate of 0.04 mm/s to the target strains.

In vitro degradation tests

In vitro degradation tests were carried out under pH 2 and pH 7 conditions. HA-Cat-NCSN hydrogels were first weighed as the original weight (m_0) and then immersed in pH 2 and pH 7 buffers and incubated at 37℃. At each time point, hydrogels were taken out from buffer and the weight was recorded as m_t. The degradation rate was determined as the ratio of the mass of hydrogels at each time point divided by the mass of as-prepared hydrogels.

Lap shear adhesion measurements

As for the lap shear test of hydrogels in between glass slides, HA-Cat and HA-NCSN were dissolved in PBS and mixed with an equal volume of MT (Sigma-Aldrich) (100 units ml^{-1} in PBS). After adding the enzyme, the mixture was vortexed immediately and applied to one end of a piece of glass. The area covered with precursor was fixed at 2.5 cm×2.5 cm. Adhesions were formed by placing a second piece of glass over the first with a 2.5 cm overlap. A similar protocol was followed for sample preparation of HA-Cat hydrogels, except that a large amount of $NaIO_4$ (1:1 $NaIO_4$: Cat molar ratio) was

used for HA-Cat hydrogels to induce gelation. The adhesions were then fastened with clips, incubated at 37°C for 15 min, and then further incubated in PBS at 37°C for 0, 1, 5, or 15 min to assess its adhesive properties under wet conditions. As for the lap shear hydrogels in between porcine gastric tissues, the porcine gastric tissues were preliminarily cutting into similar size (fixed at 2.5 cm×2.5 cm) and glued firmly to the glass slides. HA-Cat and HA-NCSN were dissolved in PBS and mixed with an equal volume of MT (Sigma-Aldrich) (100 units ml^{-1} in PBS). After adding the enzyme, the mixture was vortexed immediately and applied to the tissue surface on the slides. Adhesions were formed by placing another piece of gastric tissue-attached slide over the first. The adhesions were then fastened with clips, incubated at 37°C for 15 min, and then further incubated in acidic gastric medium at 37°C overnight to assess its adhesive properties. The samples were pulled to failure using a tensile testing machine with a speed of 1 mm/min at room temperature. The load and displacement were recorded.

Animal experiment design

All the animal handling procedures have been approved by the Animal Experimentation Ethics Committee (AEEC) of The Chinese University of Hong Kong (No. 15-178-MIS and 15-025-MIS).

Efficacy of the hydrogel in treating gastric ulcer in a rodent model

Sprague Dawley (SD) rats weighing 200 to 250 g (n=6, female) were provided by the Laboratory Animal Services Centre of CUHK for this study. A rodent model of acetic acid-induced gastric ulcers was established using a previously reported protocol (*58*). After a 24 h fast, rats were anaesthetized by an intraperitoneal injection of ketamine (80 mg/kg body weight). The stomach was then isolated. A hollow O-ring mold (OD=10 mm) with an inlet and outlet was placed in the gastric body through a small incision at the fundus region. The mold was gripped tightly by the surgeon's fingers, and 75% acetic acid was injected into the mould through the inlet. After 90 seconds, two symmetric gastric ulcers were created on the anterior and posterior walls of the stomach (Fig. 4A). Next, DPBS (Dulbecco's phosphate-buffered saline, Sigma-Aldrich) was

injected to wash away the excess acid. After the ulcers were created, two symmetric gastric ulcers in one stomach were divided into the hydrogel group (ulcers on the anterior wall) and control group (ulcers on the posterior wall). For the hydrogel group, precursor mixtures of 2% HA-Cat and 2% HA-NCSN were applied to the ulcers, and a low concentration of oxidant with a 0.1:1 $NaIO_4$: catechol ratio was sprayed onto the precursor to induce gelation using the same methods as described for the pig study. No treatment was applied to the control group. Stomach samples were collected on day 7. The surface area of gastric ulcers on the anterior and posterior walls of the stomach from each of 6 rats was assessed. The ulcer tissues were then fixed with formalin for 24 h and embedded in paraffin for histological analysis.

Endoscopic procedures of hydrogel precursor and drug delivery to treat ulcer in a porcine model

Pigs weighing 20-25 kg were used in this study. ESD was performed at the body of the stomach to create three ulcers, each about 1 cm in diameter. A gastroscope (HQ190; Olympus) with a fitted disposable distal attachment cap was used for ESD. An electrosurgical unit (VIO 300D; ERBE Elektromedizin) was used for electrical cutting and coagulation. Pigs with artificial ulcers were randomly assigned to one of three groups: the control group, the drug treatment group, and the hydrogel group. For the hydrogel group, a precursor mixture of 2% HA-Cat and 2% HA-NCSN containing blue dye (Brilliant Blue FCF) was initially applied to the site of artificial ulcer with a catheter through the biopsy channel (catheter 1) to fully fill the defect. Another catheter (catheter 2) attached outside the scope in parallel to the biopsy channel was used to spray the same amount of a low concentration of oxidant (0.1:1 $NaIO_4$: catechol ratio, namely, 0.048% w/v) onto the hydrogel precursor. For the drug treatment group, sucralfate wrapped in gauze was delivered through endoscope and fixed at the ulcer site by endoscopic clips. For the control group, only ESD was performed and no treatment was applied. Endoscopic surveillance was performed to evaluate the ulcer healing and an endoscopic ruler was used to measure the ulcer size. Pigs were euthanized on day 14 for sample collection. The ulcer tissues were fixed with formalin for 24 h and then embedded in paraffin for the histological analysis. To assess the hydrogel retention in

vivo, one pig was induced with two ulcers at the body and antrum of the stomach, respectively. One ulcer was sprayed with hydrogel (hydrogel group) while the other served as the control without any intervention (control group). The pig received endoscopy again after 48 hours and euthanized for sample collection.

Histological analysis

H & E staining and inflammation grading

H & E staining was performed on paraffin sections of rat and porcine ulcer tissue samples. Histological features of inflammation and mucosa damage were scored according to previous literature (*41, 57*). For rat tissue sections, neutrophil infiltration was graded as follows: grade 0, no neutrophils; grade 1, <10 neutrophils/high-power field (HPF); grade 2, >10 neutrophils/HPF with infiltration limited to ≤50% of mucosal surface; grade 3, infiltration involving >50% of the mucosal surface. Lymphocyte infiltration was graded as follows: grade 0, occasional observation of lymphocytes and plasma cells; grade 1, mild focal increase in lymphocytes; grade 2, dense but focal lymphocytic infiltration; grade 3, dense and diffuse lymphocytic infiltration involving >50% of the mucosal surface. For pig tissue sections, leukocyte infiltration was graded as follows: grade 0, occasional leukocyte infiltration; grade 1, mild focal increase in leukocyte numbers; grade 2, dense but focal leukocyte infiltrate; grade 3, dense and diffuse leukocyte infiltrate involving > 50% of the mucosal surface. Architecture of glands was graded as follows: grade 0, almost normal glandular structure; grade 1, gastric glands arrange sparsely with some slightly dilated; grade 2, morphologic changes between 1 and 3; grade 3, gastric glands are dilated markedly with distorted architecture and epithelial cells are poorly differentiated.

Immunohistochemistry

Immunohistochemical staining was performed using an antibody against iNOS in pig tissue samples and antibodies against PCNA (Abcam) and CD31 (Abcam) (endothelial cell marker) in rat tissue samples. Briefly, paraffin sections (7 μm thick) of ulcer tissues were de-paraffinized and rehydrated. Next, sections were pre-digested with 0.5 mg/ml hyaluronidase for 30 min at 37°C, incubated with 0.5 N acetic acid for 4 hours at 4°C. Then, samples were incubated with 3% H_2O_2 in methanol for 10 min. Non-specific

binding was blocked by incubating samples with 10% horse serum for 20 min. Sections were then incubated overnight at 4°C with a primary antibody (iNOS 1:200, PCNA 1:3000, or CD31 1: 500) followed by incubation with a biotinylated secondary antibody. The staining was further developed using the Vectastain ABC kit (Vector Labs) and the DAB Substrate Kit (Vector Labs) for peroxidase. Additionally, sections were stained with haematoxylin before being examined under a microscope. The quantification of the percentage of PCNA-positive cells in the ulcer base and ulcer margin was calculated by the total area of DAB staining positive nucleus divided by the total area of haematoxylin staining positive nucleus.

In vitro biocompatibility test

Human mesenchymal stem cells (hMSCs) (ATCC) were expanded to passage 4 in growth media consisting of α-minimum essential medium (α-MEM) supplemented with 16.7% FBS, 1% glutamine and 1% penicillin/streptomycin. The hMSCs and human gastric epithelial cell line GES-1 cells (ATCC) were suspended at a final density of 5×10^5 cells per 50 μl of HA-Cat-NCSN hydrogel. After gelation, the hMSC-laden hydrogels and GES-1-laden hydrogels were continuously cultured in medium for 7 days, and the medium was changed every two days. The viability of cells encapsulated in hydrogels was evaluated using live/dead cell staining. The stained cells were observed using a Nikon C2+ confocal microscope, and the percent of living cells was calculated using ImageJ software (NIH).

Analysis of pepsin sequestration by hydrogels in vitro

Experiments were divided into three groups. For the HA-Cat-NCSN group, 30 μl of a precursor mixture of 2% HA-Cat and 2% HA-NCSN was applied to the bottom of the transwell chamber (corning, CNG3422), and about 30 μl of a low concentration of oxidant (0.1:1 $NaIO_4$: Cat ratio) was sprayed onto the surface to induce gelation. For the MeHA group, 60 μl of a 2% MeHA solution containing 0.05% I2959 formed a hydrogel in the transwell chamber after 20 min of UV exposure (wavelength: 365 nm, intensity: 5 mW/cm^2). Afterwards, 200 μl of a 2 mg/ml pepsin solution were added.

Chambers were then placed in wells of 24-well plates filled with 1100 μl of pH 3 buffer (fig. S13). Buffer was collected and replenished at 10 min, 30 min, 1.5 h, 3.5 h, 6 h, 10 h, 1 day, 2 days, 4 days and 7 days. The absorbance of the collected buffer was recorded at 562 nm, and the percentage of pepsin that infiltrated into lower chambers was calculated using a standard curve (fig. S13). All the chemicals were dissolved in the pH 3 buffer.

Analysis of protein absorption in hydrogel and release from hydrogels in vitro

For protein absorption, after gelation of the 2% HA-Cat and 2% HA-NCSN precursor solutions or 2% MeHA, each 50 ul hydrogel was put in 1.5 ml of 1 mg/ml BSA dissolved in pH 3 buffer. BSA solution were collected at 24 hours. For protein release, the 2% HA-Cat and 2% HA-NCSN precursor solutions or 2% MeHA solution were encapsulated with BSA to form a hydrogel with a final BSA concentration of 1 mg/ml. Then, hydrogels were incubated in pH 3 buffer. Buffer was collected and replenished at 10 min, 30 min, 1 h, 3.5 h, 7.5 h, 12 h, 1 day, 2 days, 4 days, and 7 days. The absorbance of the collected buffer was measured at 562 nm to calculate the percentage of BSA adsorbed or released using a standard curve.

In vitro culture of hGES-1 with hydrogel

hGES-1 cells were cultured in growth medium consisting of Dulbecco's Modified Eagle's Medium (DMEM, Sigma-Aldrich) supplemented with 10% FBS (fetal bovine serum, Sigma-Aldrich), 1% glutamine (Sigma-Aldrich) and 1% penicillin/streptomycin (Sigma-Aldrich). hGES-1 cells were cultured overnight, and then FGF or HA-Cat-NCSN hydrogel encapsulated with FGF (the same amount) or hydrogel pre-soaked with FGF (the same amount) were added to the dish. After 4 hours, medium in all groups were changed to growth medium, cell number was calculated at day 0, 2, 4, and 7 with three parallel samples in each group. Live/dead cell staining was performed on day 2 and day 7 according to the manufacturer's protocol, where living cells are stained green with calcein-AM, and dead cells are stained red with propidium iodide. The stained cells were observed using a Nikon C2+ confocal microscope.

RT^2 profiler PCR array

Total RNA was extracted from ulcer samples by Trizol (Invitrogen). 0.5 μg of RNA was then transcribed to cDNA using the RT^2 First Strand Kit (Qiagen). A total of 84 genes related to wound healing was examined by real-time quantitative PCR with the RT^2 profiler PCR array kit (Qiagen). Primers were provided by the kit and embedded in the 96-well plate. Settings were 95℃ for 10 minutes, and 40 cycles at 95℃ for 15 seconds and 60℃ for 1 minute. Data were analyzed through the online GeneGlobe Data Analysis Center (Qiagen). The fold change was calculated using the $2^{-\Delta\Delta Ct}$ method.

Statistical analysis

All results are presented as mean ± SEM. Normality of distributions were examined by Shapiro-Wilk test. Data were analyzed by GraphPad Prism software (GraphPad Software Inc.) by conducting paired and independent Student's *t* test for comparison between paired ulcers and the independent two groups respectively, and one-way ANOVA for comparisons across multiple groups, followed by Tukey's *post hoc* test. Two-sided $P < 0.05$ was considered statistically significant.

SUPPLYMENTARY MATERIALS

Fig. S1. ^{1}H NMR spectrum of HA-Cat.
Fig. S2. ^{1}H NMR spectrum of HA-NCSN.
Fig. S3. UV-Vis spectra of HA-Cat mixed with a 5-fold higher concentration of HA-NCSN.
Fig. S4. Mechanical comparation of HA-Cat-NCSN hydrogels and HA-Cat hydrogels.
Fig. S5. The physical properties of Ha-Cat-NCSN hydrogels.
Fig. S6. HA-Cat-NCSN hydrogels gelation induced by MT.
Fig. S7. Adhesion of HA-Cat-NCSN hydrogels on porcine gastric tissues in acidic wet environment.
Fig. S8. The gastric ulcers of rats with or without hydrogel treatment.
Fig. S9. ESD of the pig stomach.
Fig. S10. Photos and immune-staining results for iNOS of pig stomach tissue harvested 48 h post-operation.
Fig. S11. Schematic illustration of applying drugs to gastric ulcers in vivo.
Fig. S12. Biocompatibility assay of HA-Cat-NCSN.
Fig. S13. Schematic illustration of pepsin sequestration by hydrogels in an acidic

environment.
Fig. S14. BSA release test of HA-Cat-NCSN hydrogels and MeHA hydrogels.
Movie S1. Adhesive and stable hydrogels formed on the acidic and wet procine gastric tissue in vitro.
Data file S1. Individual subject-level data for quantitative analysis.

REFERENCE

1. J. Zhang, J. P. Jia, J. M. P. Kim, H. Shen, F. Yang, Q. Zhang, M. Xu, W. Z. Bi, X. Wang, J. Yang, D. C. Wu, Ionic Colloidal Molding as a Biomimetic Scaffolding Strategy for Uniform Bone Tissue Regeneration. *Advanced Materials* **29**, (2017).
2. B. Xu, P. B. Zheng, F. Gao, W. Wang, H. T. Zhang, X. R. Zhang, X. Q. Feng, W. G. Liu, A Mineralized High Strength and Tough Hydrogel for Skull Bone Regeneration. *Adv Funct Mater* **27**, (2017).
3. T. E. Brown, I. A. Marozas, K. S. Anseth, Amplified Photodegradation of Cell-Laden Hydrogels via an Addition-Fragmentation Chain Transfer Reaction. *Advanced Materials* **29**, (2017).
4. R. Mo, T. Y. Jiang, R. DiSanto, W. Y. Tai, Z. Gu, ATP-triggered anticancer drug delivery. *Nat Commun* **5**, (2014).
5. X. Zhao, J. Kim, C. A. Cezar, N. Huebsch, K. Lee, K. Bouhadir, D. J. Mooney, Active scaffolds for on-demand drug and cell delivery. *Proc Natl Acad Sci U S A* **108**, 67-72 (2011).
6. Q. Feng, J. K. Xu, K. Y. Zhang, H. Yao, N. Y. Zheng, L. Z. Zheng, J. L. Wang, K. C. Wei, X. F. Xiao, L. Qin, L. M. Bian, Dynamic and Cell-Infiltratable Hydrogels as Injectable Carrier of Therapeutic Cells and Drugs for Treating Challenging Bone Defects. *Acs Central Sci* **5**, 440-450 (2019).
7. K. Y. Zhang, Q. Feng, J. B. Xu, X. Y. Xu, F. Tian, K. W. K. Yeung, L. M. Bian, Self-Assembled Injectable Nanocomposite Hydrogels Stabilized by Bisphosphonate-Magnesium (Mg2+) Coordination Regulates the Differentiation of Encapsulated Stem Cells via Dual Crosslinking. *Adv Funct Mater* **27**, (2017).
8. Q. Feng, K. C. Wei, S. E. Lin, Z. Xu, Y. X. Sun, P. Shi, G. Li, L. M. Bian, Mechanically resilient, injectable, and bioadhesive supramolecular gelatin hydrogels crosslinked by weak host-guest interactions assist cell infiltration and in situ tissue regeneration. *Biomaterials* **101**, 217-228 (2016).
9. J. A. Yang, J. Yeom, B. W. Hwang, A. S. Hoffman, S. K. Hahn, In situ-forming injectable hydrogels for regenerative medicine. *Progress in Polymer Science* **39**, 1973-1986 (2014).
10. K. C. Wei, M. L. Zhu, Y. X. Sun, J. B. Xu, Q. Feng, S. Lin, T. Y. Wu, J. Xu, F. Tian, J. Xia, G. Li, L. M. Bian, Robust Biopolymeric Supramolecular "Host-Guest Macromer" Hydrogels Reinforced by in Situ Formed Multivalent Nanoclusters for Cartilage Regeneration. *Macromolecules* **49**, 866-875 (2016).
11. J. Sedo, J. Saiz-Poseu, F. Busque, D. Ruiz-Molina, Catechol-based biomimetic functional materials. *Adv Mater* **25**, 653-701 (2013).
12. B. P. Lee, P. B. Messersmith, J. N. Israelachvili, J. H. Waite, Mussel-Inspired Adhesives and Coatings. *Annu Rev Mater Res* **41**, 99-132 (2011).
13. N. Q. Tran, Y. K. Joung, E. Lih, K. M. Park, K. D. Park, Supramolecular Hydrogels Exhibiting Fast In Situ Gel Forming and Adjustable Degradation Properties. *Biomacromolecules* **11**, 617-625 (2010).
14. J. Shin, J. S. Lee, C. Lee, H. J. Park, K. Yang, Y. Jin, J. H. Ryu, K. S. Hong, S. H. Moon, H. M. Chung, H. S. Yang, S. H. Um, J. W. Oh, D. I. Kim, H. Lee, S. W. Cho, Tissue Adhesive Catechol-Modified Hyaluronic Acid Hydrogel for Effective, Minimally Invasive Cell Therapy. *Adv Funct Mater* **25**, 3814-3824 (2015).

15. Y. Liu, K. Ai, L. Lu, Polydopamine and its derivative materials: synthesis and promising applications in energy, environmental, and biomedical fields. *Chem Rev* **114**, 5057-5115 (2014).
16. Y. Liu, H. Meng, Z. C. Qian, N. Fan, W. Y. Choi, F. Zhao, B. P. Lee, A Moldable Nanocomposite Hydrogel Composed of a Mussel-Inspired Polymer and a Nanosilicate as a Fit-to-Shape Tissue Sealant. *Angew Chem Int Edit* **56**, 4224-4228 (2017).
17. K. Zhang, Z. Wei, X. Xu, Q. Feng, J. Xu, L. Bian, Efficient catechol functionalization of biopolymeric hydrogels for effective multiscale bioadhesion. *Mater Sci Eng C Mater Biol Appl* **103**, 109835 (2019).
18. S. Seo, S. Das, P. J. Zalicki, R. Mirshafian, C. D. Eisenbach, J. N. Israelachvili, J. H. Waite, B. K. Ahn, Microphase Behavior and Enhanced Wet-Cohesion of Synthetic Copolyampholytes Inspired by a Mussel Foot Protein. *J Am Chem Soc* **137**, 9214-9217 (2015).
19. R. Wang, J. Z. Li, W. Chen, T. T. Xu, S. F. Yun, Z. Xu, Z. Q. Xu, T. Sato, B. Chi, H. Xu, A Biomimetic Mussel-Inspired epsilon-Poly-L-lysine Hydrogel with Robust Tissue-Anchor and Anti-Infection Capacity. *Adv Funct Mater* **27**, (2017).
20. H. Lee, B. P. Lee, P. B. Messersmith, A reversible wet/dry adhesive inspired by mussels and geckos. *Nature* **448**, 338-341 (2007).
21. S. L. Zhou, Q. Chang, F. Lu, M. Xing, Injectable Mussel-Inspired Immobilization of Platelet-Rich Plasma on Microspheres Bridging Adipose Micro-Tissues to Improve Autologous Fat Transplantation by Controlling Release of PDGF and VEGF, Angiogenesis, Stem Cell Migration. *Adv Healthc Mater* **6**, (2017).
22. S. Moulay, Dopa/Catechol-Tethered Polymers: Bioadhesives and Biomimetic Adhesive Materials. *Polym Rev* **54**, 436-513 (2014).
23. H. J. Park, Y. Jin, J. Shin, K. Yang, C. Lee, H. S. Yang, S. W. Cho, Catechol-Functionalized Hyaluronic Acid Hydrogels Enhance Angiogenesis and Osteogenesis of Human Adipose-Derived Stem Cells in Critical Tissue Defects. *Biomacromolecules* **17**, 1939-1948 (2016).
24. J. Shin, E. J. Choi, J. H. Cho, A. N. Cho, Y. Jin, K. Yang, C. Song, S. W. Cho, Three-Dimensional Electroconductive Hyaluronic Acid Hydrogels Incorporated with Carbon Nanotubes and Polypyrrole by Catechol-Mediated Dispersion Enhance Neurogenesis of Human Neural Stem Cells. *Biomacromolecules* **18**, 3060-3072 (2017).
25. J. Yu, W. Wei, E. Danner, R. K. Ashley, J. N. Israelachvili, J. H. Waite, Mussel protein adhesion depends on interprotein thiol-mediated redox modulation. *Nat Chem Biol* **7**, 588-590 (2011).
26. J. Yu, W. Wei, E. Danner, J. N. Israelachvili, J. H. Waite, Effects of interfacial redox in mussel adhesive protein films on mica. *Adv Mater* **23**, 2362-2366 (2011).
27. S. C. Nicklisch, J. H. Waite, Mini-review: the role of redox in Dopa-mediated marine adhesion. *Biofouling* **28**, 865-877 (2012).
28. Y. J. Xu, K. Wei, P. Zhao, Q. Feng, C. K. Choi, L. Bian, Preserving the adhesion of catechol-conjugated hydrogels by thiourea-quinone coupling. *Biomater Sci* **4**, 1726-1730 (2016).
29. S. Hong, K. Yang, B. Kang, C. Lee, I. T. Song, E. Byun, K. I. Park, S. W. Cho, H. Lee, Hyaluronic Acid Catechol: A Biopolymer Exhibiting a pH-Dependent Adhesive or Cohesive Property for Human Neural Stem Cell Engineering. *Adv Funct Mater* **23**, 1774-1780 (2013).
30. K. S. Cheung, E. W. Chan, A. Y. S. Wong, L. Chen, I. C. K. Wong, W. K. Leung, Long-term

proton pump inhibitors and risk of gastric cancer development after treatment for Helicobacter pylori: a population-based study. *Gut* **67**, 28-35 (2018).

31. B. Bang, E. Lee, J. Maeng, K. Kim, J. H. Hwang, S. H. Hyon, W. Hyon, D. H. Lee, Efficacy of a novel endoscopically deliverable muco-adhesive hemostatic powder in an acute gastric bleeding porcine model. *PLoS One* **14**, e0216829 (2019).
32. J. H. Maeng, B. W. Bang, E. Lee, J. Kim, H. G. Kim, D. H. Lee, S. G. Yang, Endoscopic application of EGF-chitosan hydrogel for precipitated healing of GI peptic ulcers and mucosectomy-induced ulcers. *J Mater Sci-Mater M* **25**, 573-582 (2014).
33. M. Cencer, Y. Liu, A. Winter, M. Murley, H. Meng, B. P. Lee, Effect of pH on the Rate of Curing and Bioadhesive Properties of Dopamine Functionalized Poly(ethylene glycol) Hydrogels. *Biomacromolecules* **15**, 2861-2869 (2014).
34. D. G. Barrett, D. E. Fullenkamp, L. H. He, N. Holten-Andersen, K. Y. C. Lee, P. B. Messersmith, pH-Based Regulation of Hydrogel Mechanical Properties Through Mussel-Inspired Chemistry and Processing. *Adv Funct Mater* **23**, 1111-1119 (2013).
35. W. C. Schiessl, N. K. Summa, C. F. Weber, S. Gubo, C. Ducker-Benfer, R. Puchta, N. J. R. V. Hommes, R. van Eldik, Experimental and theoretical approaches to the protonation of thiourea: A convenient nucleophile in coordination chemistry revisited. *Z Anorg Allg Chem* **631**, 2812-2819 (2005).
36. H. T. Abdel-Mohsen, J. Conrad, U. Beifuss, Laccase-Catalyzed Domino Reaction between Catechols and 6-Substituted 1,2,3,4-Tetrahydro-4-oxo-2-thioxo-5-pyrimidinecarbonitriles for the Synthesis of Pyrimidobenzothiazole Derivatives. *J Org Chem* **78**, 7986-8003 (2013).
37. P. Zhao, K. Wei, Q. Feng, H. Chen, D. S. H. Wong, X. Chen, C. C. Wu, L. Bian, Mussel-mimetic hydrogels with defined cross-linkers achieved via controlled catechol dimerization exhibiting tough adhesion for wet biological tissues. *Chem Commun (Camb)* **53**, 12000-12003 (2017).
38. A. M. Jonker, A. Borrmann, E. R. van Eck, F. L. van Delft, D. W. Lowik, J. C. van Hest, A fast and activatable cross-linking strategy for hydrogel formation. *Adv Mater* **27**, 1235-1240 (2015).
39. B. P. Lee, J. L. Dalsin, P. B. Messersmith, Synthesis and gelation of DOPA-modified poly(ethylene glycol) hydrogels. *Biomacromolecules* **3**, 1038-1047 (2002).
40. N. Annabi, Y. N. Zhang, A. Assmann, E. S. Sani, G. Cheng, A. D. Lassaletta, A. Vegh, B. Dehghani, G. U. Ruiz-Esparza, X. Wang, S. Gangadharan, A. S. Weiss, A. Khademhosseini, Engineering a highly elastic human protein-based sealant for surgical applications. *Sci Transl Med* **9**, (2017).
41. X. Xia, P. W. Y. Chiu, P. K. Lam, W. C. Chin, E. K. W. Ng, J. Y. W. Lau, Secretome from hypoxia-conditioned adipose-derived mesenchymal stem cells promotes the healing of gastric mucosal injury in a rodent model. *Biochim Biophys Acta Mol Basis Dis* **1864**, 178-188 (2018).
42. A. Tarnawski, J. Stachura, W. J. Krause, T. G. Douglass, H. Gergely, Quality of gastric ulcer healing: a new, emerging concept. *J Clin Gastroenterol* **13 Suppl 1**, S42-47 (1991).
43. Y. Hayashi, S. Tsuji, M. Tsujii, T. Nishida, S. Ishii, H. Iijima, T. Nakamura, H. Eguchi, E. Miyoshi, N. Hayashi, S. Kawano, Topical transplantation of mesenchymal stem cells accelerates gastric ulcer healing in rats. *Am J Physiol Gastrointest Liver Physiol* **294**, G778-786 (2008).

44. G. K. Dudar, L. D. D'Andrea, R. Di Stasi, C. Pedone, J. L. Wallace, A vascular endothelial growth factor mimetic accelerates gastric ulcer healing in an iNOS-dependent manner. *Am J Physiol Gastrointest Liver Physiol* **295**, G374-381 (2008).
45. B. Steffensen, L. Hakkinen, H. Larjava, Proteolytic events of wound-healing-coordinated interactions among matrix metalloproteinases (MMPs), integrins, and extracellular matrix molecules. *Crit Rev Oral Biol M* **12**, 373-398 (2001).
46. N. Ferrara, Vascular endothelial growth factor: basic science and clinical progress. *Endocr Rev* **25**, 581-611 (2004).
47. M. R. Alison, R. Chinery, R. Poulsom, P. Ashwood, J. M. Longcroft, N. A. Wright, Experimental ulceration leads to sequential expression of spasmolytic polypeptide, intestinal trefoil factor, epidermal growth factor and transforming growth factor alpha mRNAs in rat stomach. *J Pathol* **175**, 405-414 (1995).
48. K. Magierowska, D. Bakalarz, D. Wojcik, A. Chmura, M. Hubalewska-Mazgaj, S. Licholai, E. Korbut, S. Kwiecien, Z. Sliwowski, G. Ginter, T. Brzozowski, M. Magierowski, Time-dependent course of gastric ulcer healing and molecular markers profile modulated by increased gastric mucosal content of carbon monoxide released from its pharmacological donor. *Biochem Pharmacol* **163**, 71-83 (2019).
49. J. H. Lee, J. Y. Jung, D. Bang, The efficacy of topical 0.2% hyaluronic acid gel on recurrent oral ulcers: comparison between recurrent aphthous ulcers and the oral ulcers of Behcet's disease. *J Eur Acad Dermatol Venereol* **22**, 590-595 (2008).
50. A. Schmassmann, A. Tarnawski, B. M. Peskar, L. Varga, B. Flogerzi, F. Halter, Influence of acid and angiogenesis on kinetics of gastric ulcer healing in rats: interaction with indomethacin. *Am J Physiol* **268**, G276-285 (1995).
51. A. H. Soll, J. H. Walsh, Regulation of gastric acid secretion. *Annu Rev Physiol* **41**, 35-53 (1979).
52. S. Ebnesajjad, ADHESIVES TECHNOLOGY HANDBOOK Second Edition Preface. *Adhesives Technology Handbook, 2nd Edition*, Xix-Xxi (2009).
53. M. Szura, A. Pasternak, Upper non-variceal gastrointestinal bleeding - review the effectiveness of endoscopic hemostasis methods. *World J Gastro Endos* **7**, 1088-1095 (2015).
54. M. Bustamante-Balen, G. Plume, Role of hemostatic powders in the endoscopic management of gastrointestinal bleeding. *World J Gastrointest Pathophysiol* **5**, 284-292 (2014).
55. J. Su, F. Chen, V. L. Cryns, P. B. Messersmith, Catechol polymers for pH-responsive, targeted drug delivery to cancer cells. *J Am Chem Soc* **133**, 11850-11853 (2011).
56. J. Xu, S. Strandman, J. X. Zhu, J. Barralet, M. Cerruti, Genipin-crosslinked catechol-chitosan mucoadhesive hydrogels for buccal drug delivery. *Biomaterials* **37**, 395-404 (2015).
57. X. F. Xia, K. F. Chan, G. T. Y. Wong, P. Wang, L. Liu, B. P. M. Yeung, E. K. W. Ng, J. Y. W. Lau, P. W. Y. Chiu, Mesenchymal stem cells promote healing of nonsteroidal anti-inflammatory drug-related peptic ulcer through paracrine actions in pigs. *Science Translational Medicine* **11**, (2019).
58. S. Okabe, K. Amagase, An overview of acetic acid ulcer models--the history and state of the art of peptic ulcer research. *Biol Pharm Bull* **28**, 1321-1341 (2005).

Acknowledgements: The authors would like to thank Y. Tang from the Konstfack -

University of Arts, Crafts and Design for her help in conducting the original and fine hand-drawn illustration of the stomach shown in Fig. 5. The authors would also like to thank Dr. Q. Feng, Dr. H. Chen, Dr. R. Li, Dr. X. Yan and Mr. Y. Xu for participating in valuable discussions. **Funding:** This project is supported by Innovation and Technology Fund of Hong Kong (ITS/246/17 to P.W.-Y.C.), the National Natural Science Foundation of China (31570979 to L. B.), the General Research Fund grant from the Research Grants Council of Hong Kong (14220716 to L. B.), the Health and Medical Research Fund of The Food and Health Bureau of Hong Kong (04152836 to L. B.). Chow Yuk Ho Technology Centre for Innovative Medicine of The Chinese University of Hong Kong provided the support on animal experiments. **Author contributions:** L.B. and P.W.-Y.C. provided the funding. L.B., P. W.-Y.C., X. Xu, X. Xia, and K. Z. conceived the idea and designed the experiments. K. W. and P. Z. contributed to the research design. X. Xu and K. Z. led and performed the majority of the in vitro experiments. B. Y., Z. L. and W.-K. W. participated in polymer synthesis. X. Xia performed the animal experiments with the help of X. Xu, K. Z., A. R. and L. Z. X. Xu and X. Xia collected and analysed the data. X. Xu drafted the manuscript. L. B., K. Z., and X. Xia revised the paper. **Competing interests:** L.B., P.Z., and K.W. are inventors on patent US10208104B2 held by the Chinese University of Hong Kong that covers the “fast and efficient conjugation method based on thiourea-catechol coupling”, which was used to fabricate the hydrogels used in the current work. A US patent has been filed for this work (US 2017/0204161A1). The authors declare that they have no competing interests. **Data and materials availability:** All data associated with this study are present in the paper or in the Supplementary Materials.

Figure Legends

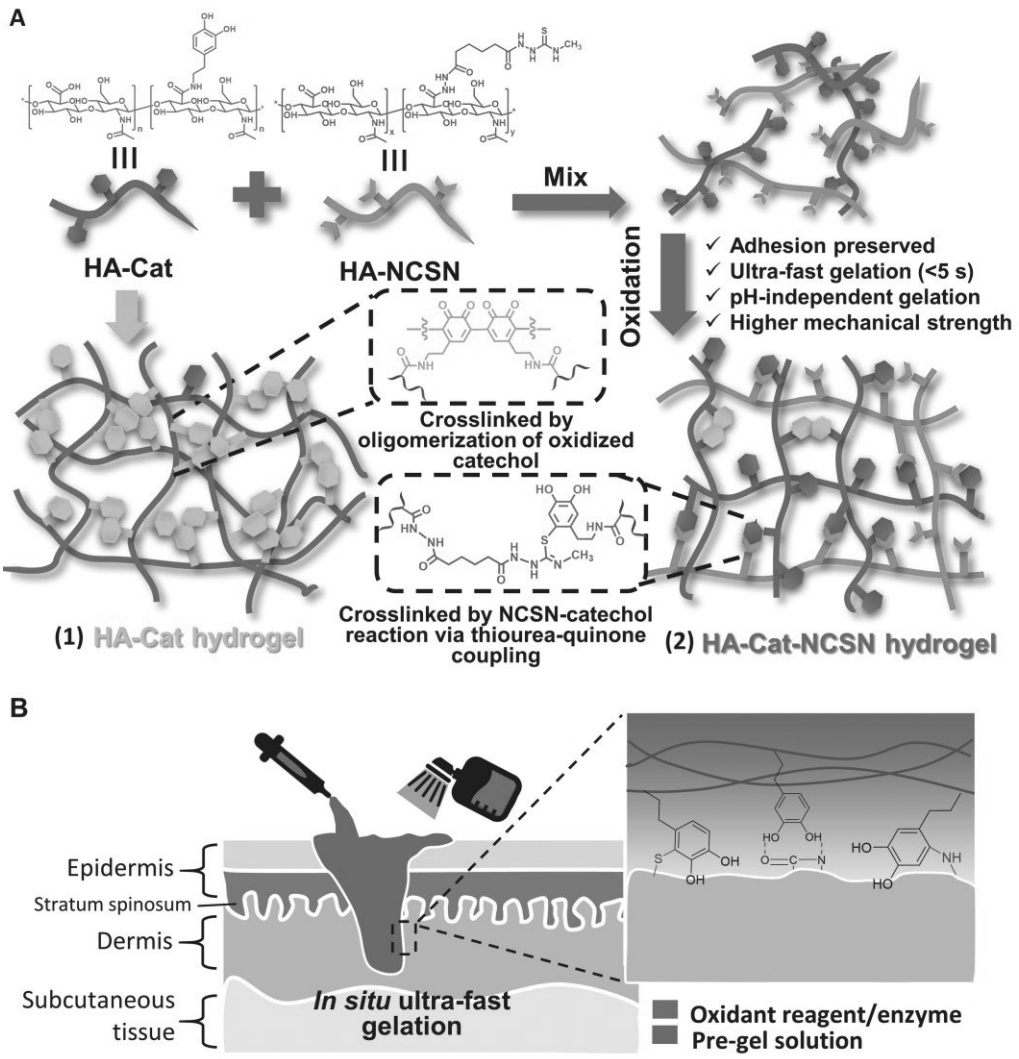

Fig. 1. Schematic illustration of the fabrication process and mechanisms of bio-adhesion. (**A**) Schematic illustrating the fabrication process and putative crosslinked structure of HA-Cat and HA-Cat-NCSN hydrogels. (**B**) Schematic illustrating a HA-Cat-NCSN hydrogel formed in situ in the stomach by spraying oxidant to the precursor solution, and the mechanisms of bio-adhesion induced by the binding of abundant Cat groups in the hydrogel network to proteins on the tissue surface.

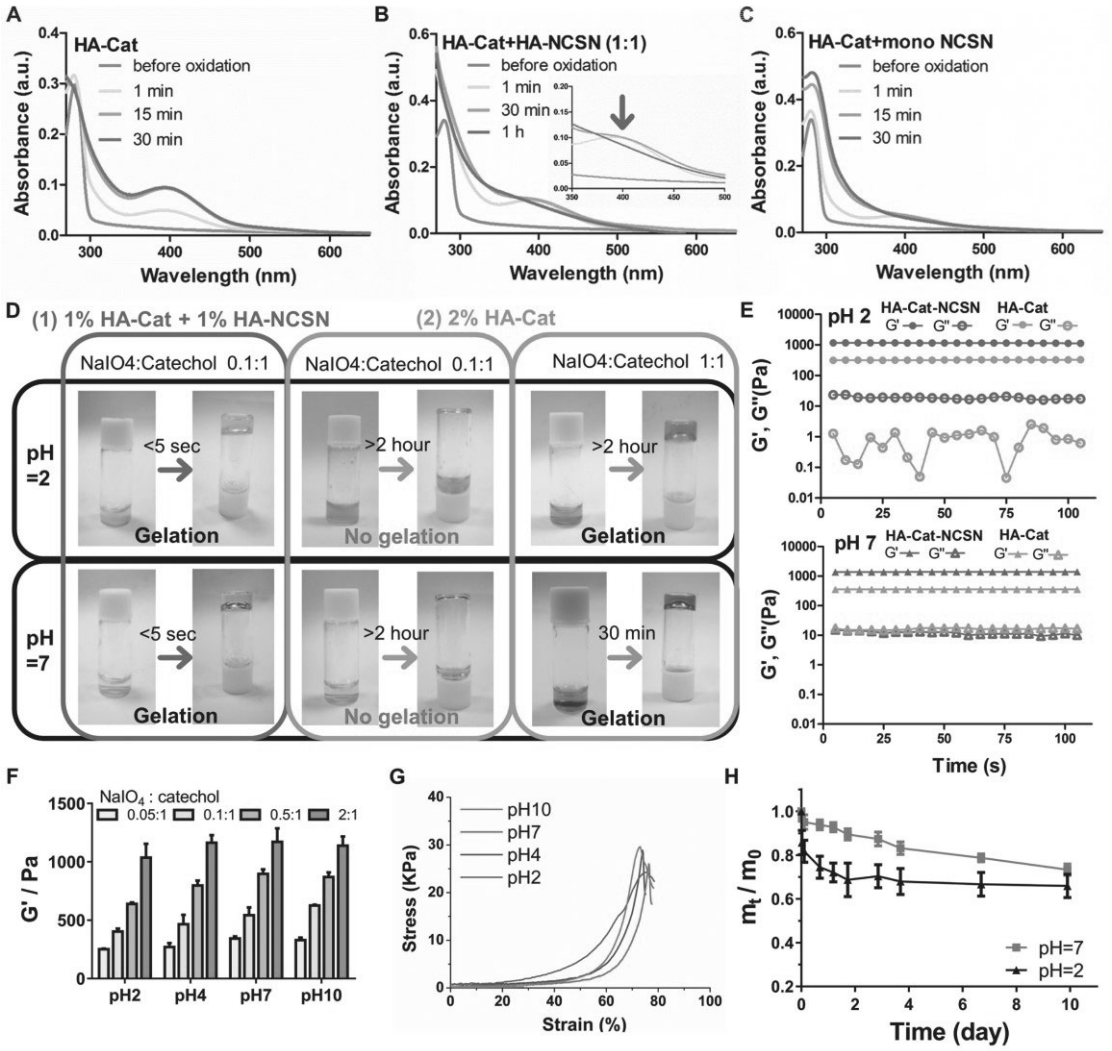

Fig. 2. HA-Cat-NCSN hydrogels demonstrate pH independence, superior mechanical properties, and instant in situ gelation in a wet and acidic environment. UV-Vis spectra of HA-Cat (**A**) and HA-Cat mixed with HA-NCSN (**B**) or monomer NCSN (**C**). The quinone peak is shown by blue arrow (λ_{max}=395 nm). (**D**) Photographs showing the gelation behaviors of HA-Cat-NCSN and HA-Cat hydrogels. (**E**) Storage modulus (G') and loss modulus (G'') of HA-Cat-NCSN and HA-Cat hydrogels at pH 2 and pH 7 recorded in the time sweep test (1:1 $NaIO_4$: Cat molar ratio). (**F**) Average elastic modulus of HA-Cat-NCSN hydrogel formed at different pH and molar ratio between $NaIO_4$ and Catechol (n=3). (**G**) Compression test for hydrogels formed at different pH (1:10 $NaIO_4$: Cat molar ratio). (**H**) Degradation of hydrogels in buffer of pH 7 and 2 for 10 days, with m_0 represents the weight of original as-prepared hydrogels and m_t represents the weight of hydrogels at specific time point (n=3). Data are

presented as means ± SEM.

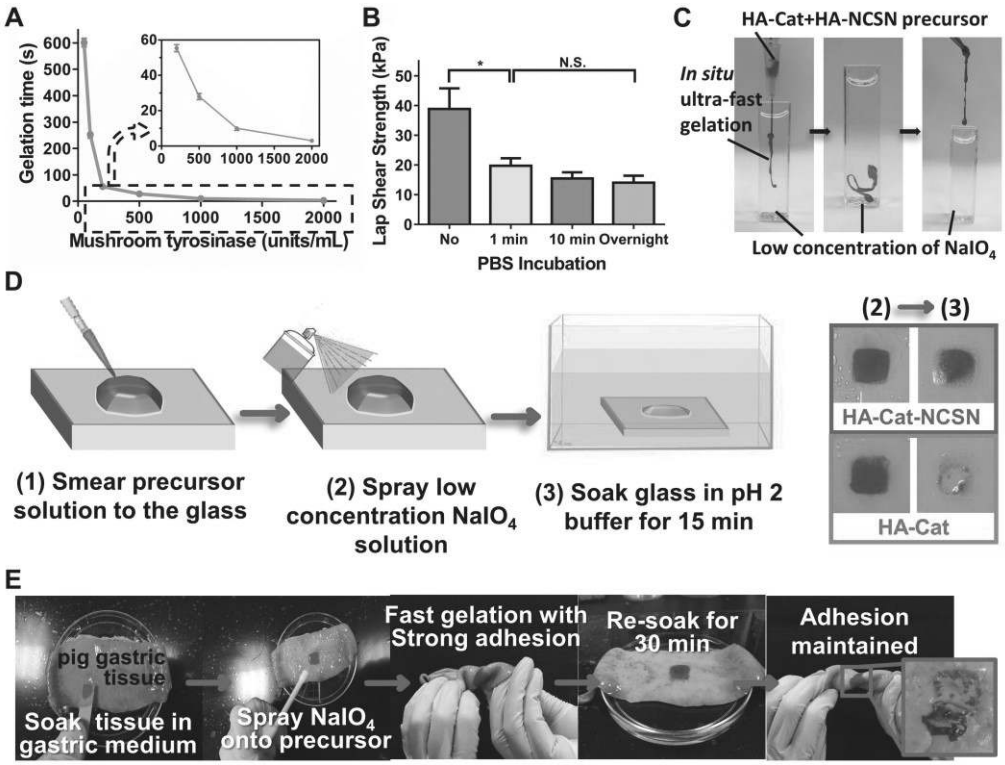

Fig. 3. HA-Cat-NCSN hydrogels demonstrate instant in situ gelation on glass and gastric tissue in wet and acidic environments. (**A**) Gelation time of HA-Cat-NCSN hydrogels prepared with different concentrations of MT (n=3). (**B**) Average adhesion strength for hydrogels (prepared with MT) after incubating in PBS for 0, 1, 10 min, or overnight (n=3). (**C**) Photos of ultrafast gelation of HA-Cat-NCSN hydrogels by directly injecting a precursor solution into the oxidant solution to form a thread-like hydrogel. (**D**) Schematic of hydrogels prepared by applying precursor solution on glass slides and spraying oxidant solution on top before soaking the glass in buffer. Photos of gels are shown on the right. (**E**) Photos of adhesive and stable hydrogels formed on a fresh, wet pig gastric tissue in vitro. Statistical significance was calculated by one-way analysis of variance (ANOVA) with the Tukey's post hoc test. $^{N.S.}P > 0.05$, $^{*}P < 0.05$, $^{**}P < 0.01$. Data are presented as means ± SEM.

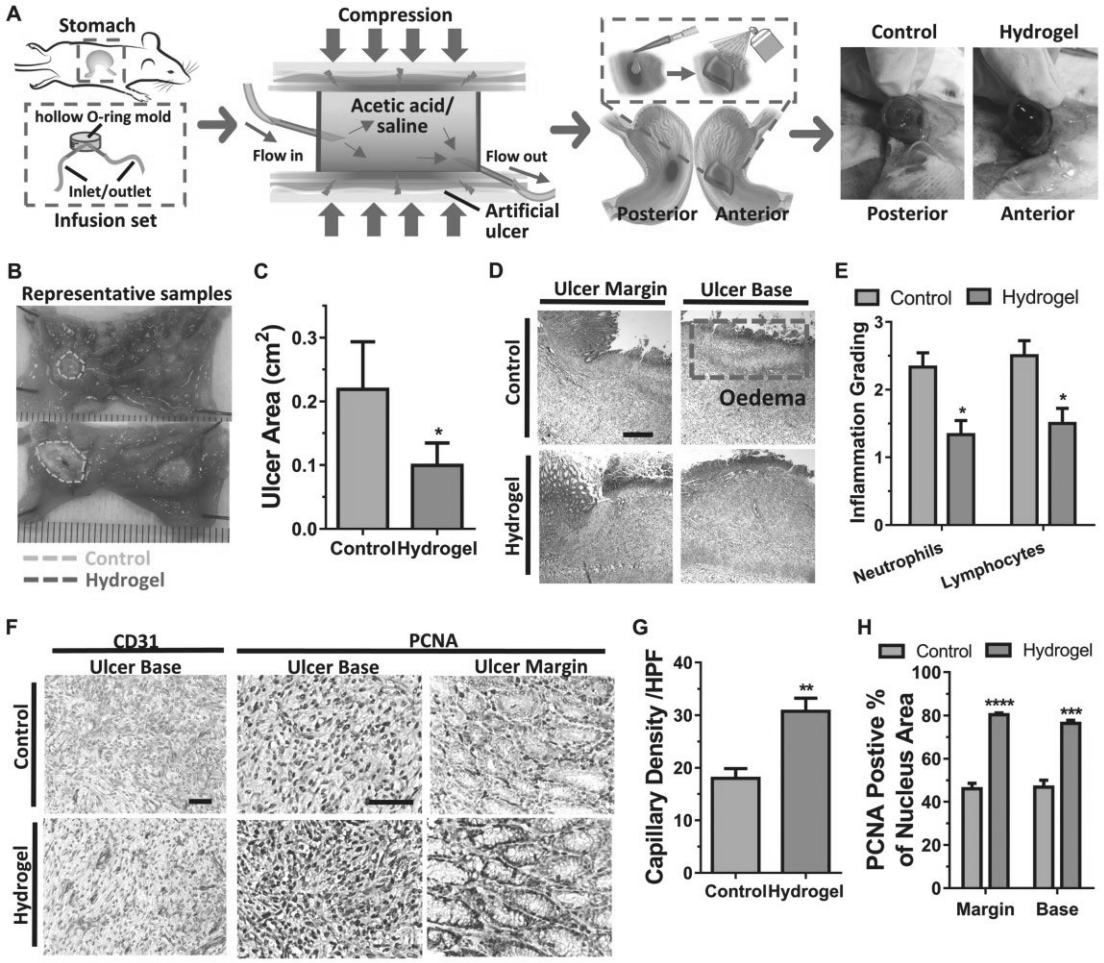

Fig. 4. Ulcer healing by the application of HA-Cat-NCSN hydrogel which suppresses inflammation and promotes angiogenesis and cell proliferation. (**A**) Schematic plot illustrating the procedures to establish kissing gastric ulcers in rats and application of HA-Cat-NCSN hydrogels on ulcer surface. Photographs are shown at far right. (**B**) Representative macroscopic images of kissing gastric ulcers in the posterior and anterior wall of the stomach in rats at day 7. (**C**) The area of gastric ulcers in the control group and hydrogel treatment group. (**D**) Microscopic images of H & E staining (Scale bar, 500 μm). (**E**) Histopathological evaluation of inflammation in ulcers obtained on day 7 based on neutrophil and lymphocyte infiltration. (**F**) Immunohistochemistry for CD31 (20×) and PCNA (40×) (Scale bar, 75 μm) of the gastric ulcer sections in each group. (**G**) Quantification of CD31-positive capillaries per high-power field (HPF). (**H**) Quantification of the percentage of PCNA-positive cells in the ulcer base and around ulcer margin. Rats, n=6. Statistical significance was calculated by Student's *t* test. $^{N.S.}P > 0.05$, $^{*}P < 0.05$, $^{**}P < 0.01$, $^{***}P < 0.001$ and $^{****}P$

< 0.0001. Data are presented as means ± SEM.

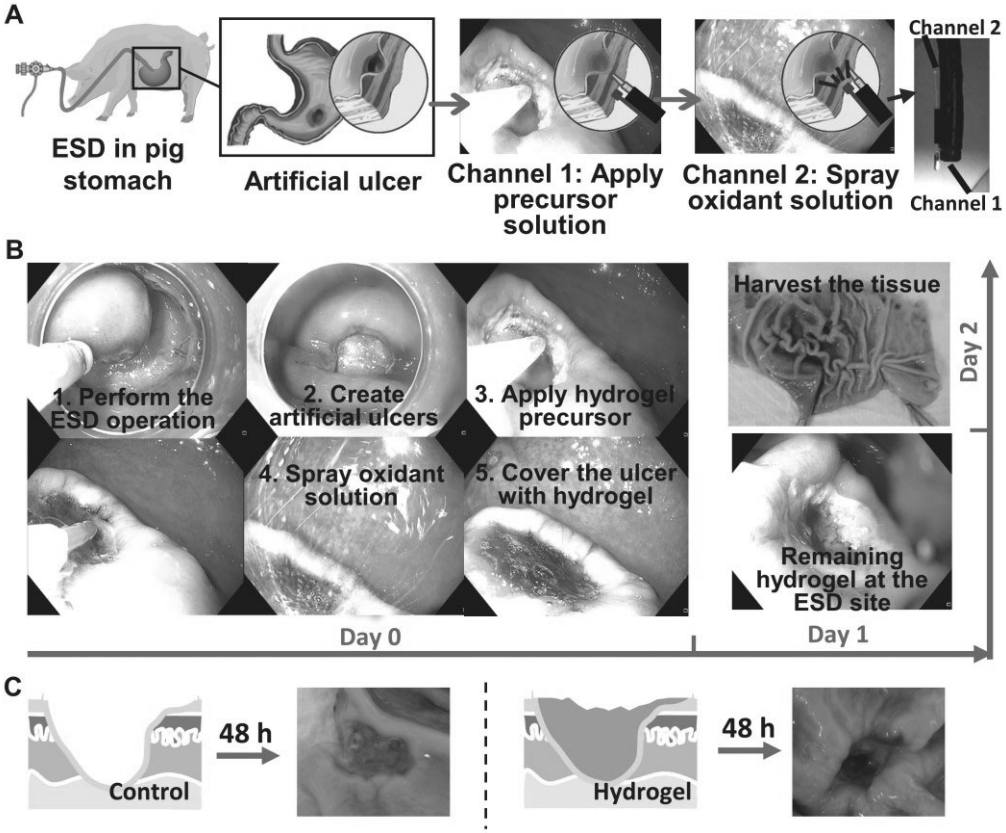

Fig. 5. In Situ ultrafast gelation of HA-Cat-NCSN hydrogel at gastric ulcer sites in a porcine model. (**A**) Schematic illustration of the process by which HA-Cat-NCSN hydrogels were applied on the gastric ulcers induced by endoscopic submucosal dissection (ESD) in pigs through endoscopic catheters. A photograph of the catheters is shown at far right. (**B**) Endoscopic imaging of the procedure of creating artificial ulcers by ESD, spraying hydrogels, and endoscopic surveillance on the gel retention at the ulcer sites after 24 and 48 hours post-operation. (**C**) Macroscopic images of pig stomach tissue harvested after 48 hours post-operation.

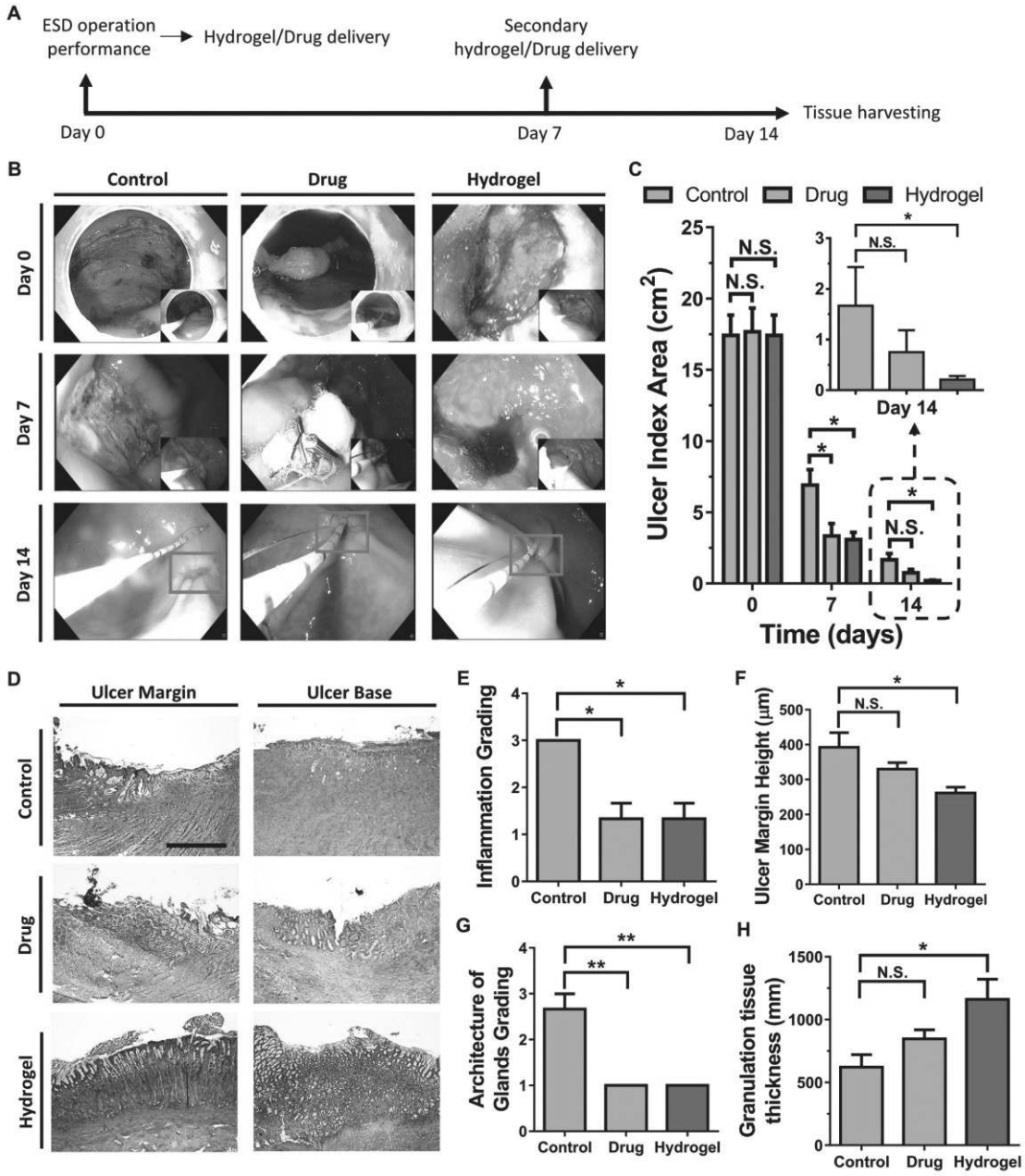

Fig. 6. HA-Cat-NCSN hydrogel treatment promotes gastric ulcer healing in vivo. (**A**) The timeline for the pig experiment. The pigs received hydrogel or drug treatment twice on day 0 and day 7, respectively. Gastric tissues of the pigs were harvested on day 14. (**B**) Endoscopic images of gastric ulcers on day 0, 7, and 14 in each group. (**C**) The ulcer index was calculated as the product of the longest and shortest radius of the ulcers. (**D**) Microscopic images of H & E staining of stomach sections on day 14 in each group. Photos were taken from ulcer margin and ulcer base (Scale bar, 1 mm). (**E** to **H**) Histological evaluation of stomach sections based on the scoring of inflammation, ulcer margin height, architecture of glands and granulation tissue thickness. Pigs, n=3.

Statistical significance was calculated by one-way analysis of variance (ANOVA) with the Tukey's *post hoc* test. $^{N.S.}P > 0.05$, $^{*}P < 0.05$, $^{**}P < 0.01$. Data are presented as means ± SEM.

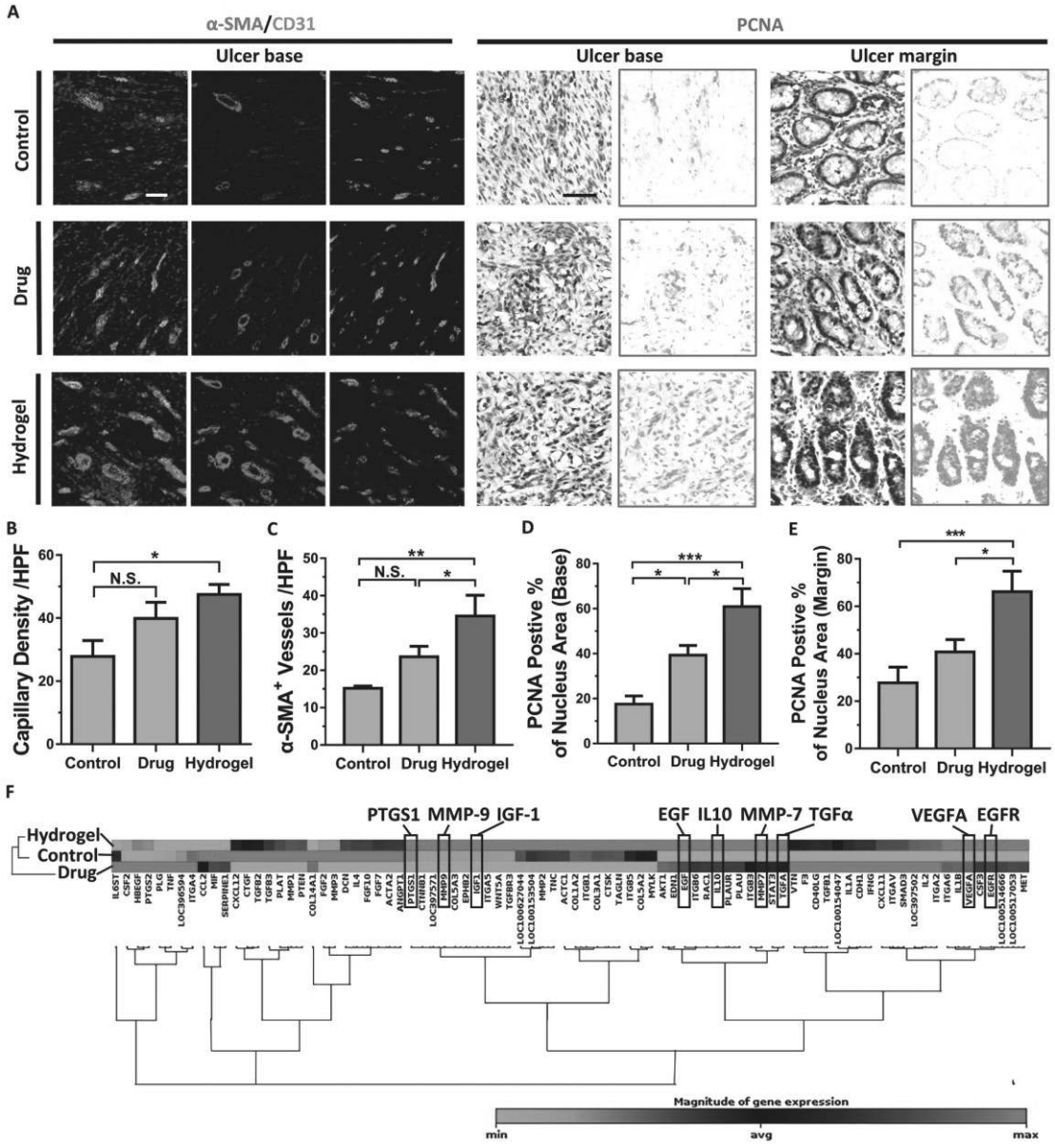

Fig. 7. Hydrogel treatment enhances cell proliferation and angiogenesis and upregulates genes associated with wound healing in pigs. (**A**) Immunostaining for CD31 (green, 20x), α-smooth muscle actin (α-SMA, red) and PCNA (dark brown nuclei, 40×) of gastric ulcer sections following treatment with hydrogels, sucralfate, and the control (no treatment). Scale bar, 50 μm. (**B**) Quantification of CD31-positive capillaries and (**C**) α-SMA-positive small arteries per high-power field (HPF).

Quantification of the percentage of PCNA-positive cells in the ulcer base (**D**) and around ulcer margin (**E**). (**F**) RT^2 profiler PCR array showing the upregulation of genes critical to wound healing after applying the hydrogel compared with the drug treatment group and control group on day 7. Pigs, n=3. Statistical significance was calculated by one-way analysis of variance (ANOVA) with the Tukey's *post hoc* test. $^{N.S.}P > 0.05$, $^{*}P < 0.05$, $^{**}P < 0.01$, $^{***}P < 0.001$. Data are presented as means ± SEM.

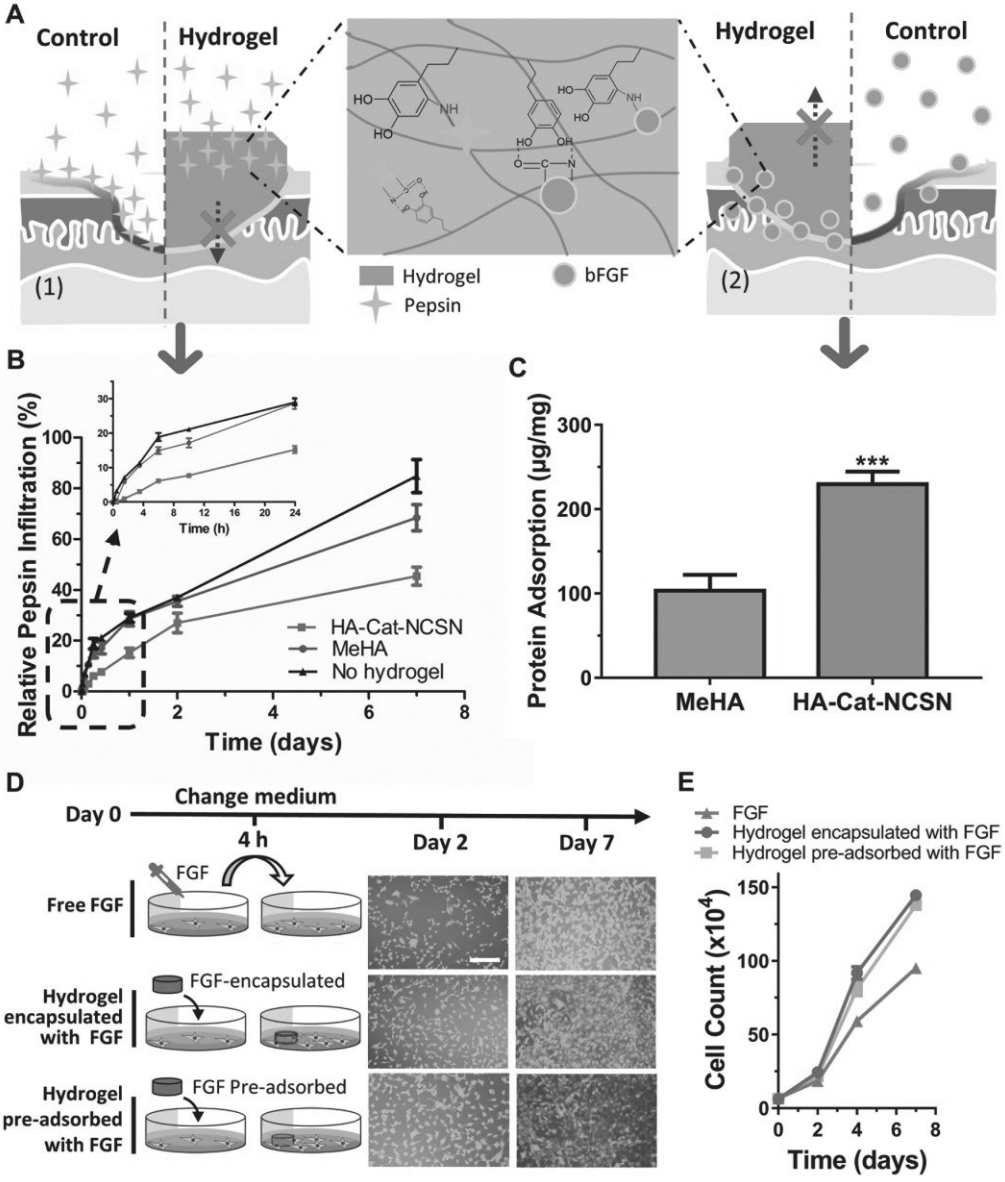

Fig. 8. HA-Cat-NCSN hydrogels promote ulcer healing by sequestration of biomolecules. (**A**) Schematic illustration of the hypothesis that the in situ-formed HA-Cat-NCSN hydrogel can prevent pepsin from diffusing to the ulcer defect and retain the

cell-secreted bFGF in the area of the ulcer defect. (**B**) Cumulative percentage of pepsin diffusing from the upper chamber into the lower chamber through a transwell system coated with HA-Cat-NCSN, MeHA, or nothing over 7 days (n=3). (**C**) The BSA absorption capacity of HA-Cat-NCSN hydrogel or the MeHA hydrogel after 24 hours incubation in BSA acidic solution (n=3). (**D**) Schematic illustration and live/dead staining image of GES-1 cells in 3 treatment groups (Scale bar, 200 μm). For the control group, 0.2 μg FGF was added directly to the culture dish containing GES-1 cells. For the experimental groups, each hydrogel was encapsulated with 0.2 μg FGF or pre-adsorbed in FGF solution containing 0.2 μg FGF for 24 hours before being added to the culture dish. (**E**) Number of GES-1 cells collected on day 0, 2, 4, and 7 in each group (n=3). Statistical significance was calculated by Student's *t* test. $^{***}P < 0.001$. Data are presented as means ± SEM.